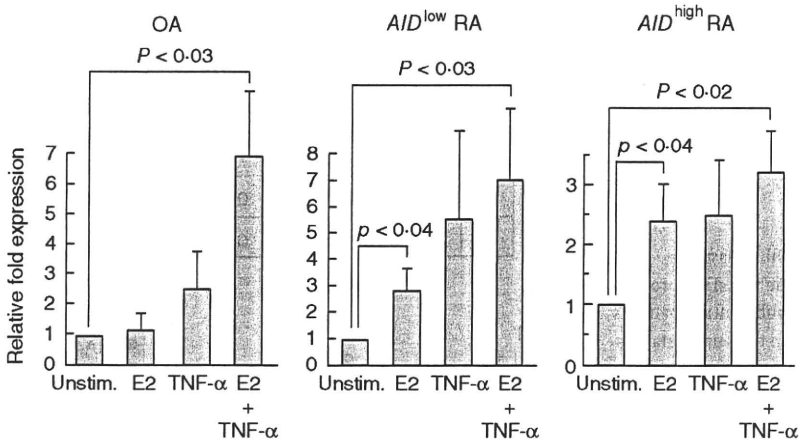

Fig. 2. Inducible expression of *AID* in transformed fibroblast-like synoviocytes (FLS) lines by stimulation with tumour necrosis factor (TNF)-α and oestrogen. One million osteoarthritis (OA)-FLS (OA2, OA6 and OA9), *AID*^{low} RA-FLS (RA2, RA3 and RA6) and *AID*^{high} RA-FLS (RA1, RA4 and RA7) were stimulated in phenol red-free Dulbecco's modified Eagle's complete medium (DMEM) with either TNF-α (50 ng/ml) or β-oestradiol (E_2; 10^{-9} M) for 24 h. The *AID* transcription was quantified (relative quantification) by real-time polymerase chain reaction (PCR) and normalized to the housekeeping gene, *GAPDH* and the relative fold induction over the unstimulated cells (Unstim.) was monitored by the ΔΔCT method. The grey bars and error bars indicate the averages and standard deviations, respectively, of three cell lines. *P*-values calculated by Student's *t*-test are indicated.

with that of *AID* (data not shown), suggesting that *AID* transcription is induced passively by external stimuli present most commonly in RA rather than that provided by inflammatory cytokines in an autocrine fashion.

Accumulation of *TP53* gene mutations in AID-expressing RA-FLS

Detailed studies have established that the mutations of the p53 tumour suppressor gene found in RA-FLS could contribute to both the tumour-like and proinflammatory properties of RA-FLS, such as aggressive growth, invasion and destruction of cartilage and bone [15–19,21–23]. Although genotoxic and oxidative stresses have been speculated to be the causative candidates for the somatic mutation in the *TP53* gene in RA-FLS, the molecular mechanism has not yet been elucidated. Recently, a clear relationship between AID expression and the frequency of *TP53* somatic mutations has been demonstrated in some non-B lymphocytes, such as hepatocytes and colon epithelial cells [29–33]. To investigate whether this is the case for RA-FLS, the coding region of *TP53* was amplified by RT–PCR with high-fidelity polymerase, sequenced and then compared among OA-FLS, *AID*^{low} RA-FLS and *AID*^{high} RA-FLS. The frequency of *TP53* somatic mutations was elevated significantly in *AID*^{high} RA-FLS rather than in OA-FLS and *AID*^{low} RA-FLS (summarized in Table 2). Although sporadic mutations were detected even in the latter two FLS, *AID*^{high} RA-FLS exhibited approximately two- to 3·5-fold more mutations than the other two FLS subsets. In addition, the frequency of non-

Table 2. Mutation frequency of TP53.

	Number of base substitution	Total base pair of sequenced	Frequency/10 000	Mutation		
				Silent	Missense	Non-sense
OA2	0	23 587	0	0	0	0
OA6	0	25 150	0	0	0	0
OA9	1	27 146	0·368	1	0	0
RA2	2	22 456	0·891	2	0	0
RA3	1	29 459	0·339	0	1	0
RA6	2	24 631	0·812	1	1	0
RA1	8	26 187	3·054	2	6	0
RA4	6	26 655	2·251	2	4	0
RA7	4	23 657	1·691	0	3	1

cDNA was prepared from representative fibroblast-like synoviocyte (FLS) lines in each group. Osteoarthritis (OA)-FLS: OA2, OA6 and OA9. Activation-induced cytidine deaminase (AID)^{low} rheumatoid arthritis (RA)-FLS: RA2, RA3 and RA6. AID^{high} RA-FLS: RA1, RA4 and RA7. The coding region of *TP53* ranging from exons 4–11 was amplified using high-fidelity DNA polymerase. Mutation frequency was analysed by sequencing of polymerase chain reaction product.

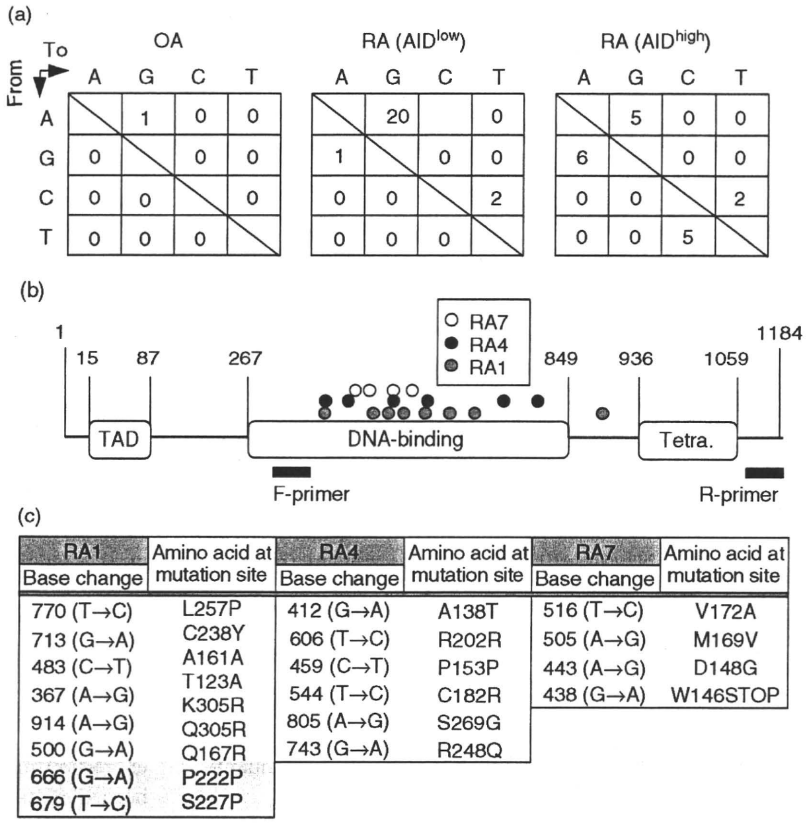

(c)

RA1		RA4		RA7	
Base change	Amino acid at mutation site	Base change	Amino acid at mutation site	Base change	Amino acid at mutation site
770 (T→C)	L257P	412 (G→A)	A138T	516 (T→C)	V172A
713 (G→A)	C238Y	606 (T→C)	R202R	505 (A→G)	M169V
483 (C→T)	A161A	459 (C→T)	P153P	443 (A→G)	D148G
367 (A→G)	T123A	544 (T→C)	C182R	438 (G→A)	W146STOP
914 (A→G)	K305R	805 (A→G)	S269G		
500 (G→A)	Q305R	743 (G→A)	R248Q		
666 (G→A)	Q167R				
679 (T→C)	P222P				
	S227P				

Fig. 3. *TP53* mutations in fibroblast-like synoviocytes (FLS). (a) Gene mutation profiles of *TP53* in FLS lines. Base substitution patterns seen in *TP53* extracted from the same data sets as those used for the mutation frequency analysis in Table 1 are shown. The numbers in the box are the sum of three FLS lines in each group. (b) Distribution of gene mutations in *TP53* from FLS lines. Each number in the figure corresponds to the position of nucleotide on the coding sequence of *TP53*. Open circles are from RA7, filled circles are from RA4 and grey circles are from RA1. The location of polymerase chain reaction (PCR) primers used for sequencing is also depicted. TAD: transactivation domain; Tetra. tetramerization domain. (c) Base and amino acids substitution in *TP53* from three of AID^{high} RA-FLS lines. Amino acids are described in a single letter. The two shaded mutations in RA1 were double mutations found in one clone.

silent mutations was three times greater than that of silent mutations. Notably, the dominant base substitution pattern is the transition type, which is very similar to the mutations found at the variable region of the immunoglobulin gene, introduced exclusively by AID (Fig. 3a) [26]. Introduction of somatic mutations at the Ig variable region by AID is coupled with the transcription level of the *Ig* gene [38] because AID attacks the single-strand DNA that appears at transcription. Thus, the somatic mutation requires both the expression of AID and the transcription of the target gene. Among the representative FLS lines, *TP53* was transcribed constitutively and the amounts of *TP53* mRNA were comparable, indicating that the increased frequency of mutation in *TP53* resulted mainly from *AID* expression rather than the transcription levels of *TP53* (data not shown). Compared with *TP53* mutations in previous reports [15,18,19,22], 17% of the mutations that we identified resulted in the changes of amino acids identical with those and 33% of those in different amino acids, but were located at the same codon. The non-sense mutation in RA7 in this study occurred at the same position as that reported by Yamanishi *et al.* [22].

While the sequencing range did not cover the whole coding sequence of *TP53*, the mutations in the *TP53* gene were obviously concentrated at the DNA-binding domain, which is the hotspot of somatic mutations found in some malignant tumours (Fig. 3b). In particular, the Arg^{248} mutation found in RA4 has been reported as one of the cancer hotspot mutations [39]. The details of both base and amino acid substitutions are listed in Fig. 3c. These data indicate that AID^{high} RA-FLS have higher frequencies of *TP53* mutations, some of which could result in the loss of function of TP53.

AID is expressed by non-transformed RA-FLS and in the RA-synovium outside of the B cell follicles

To address the issue of whether the aberrant expression of AID is affected by the transformation with SV40 large T antigen, first we examined the endogenous AID expression in non-transformed primary cell lines of FLS. *AID* transcription was detectable in four of 11 primary RA-FLS at three to eight times higher levels compared to transformed OA-FLS, but in none of six primary OA-FLS (Fig. 4a, and data not shown), indicating that increased expression of *AID* in RA-FLS is independent of transformation with SV40 large T antigen.

We then examined the production of AID protein in non-transformed RA-FLS. Cytostaining with two different anti-AID antibodies clearly exhibited the production of AID protein in AID^+ primary RA-FLS (Fig. 4b, i and ii corresponding to pRA5) but not in AID^- primary OA-FLS (Fig. 4b, iii and iv, corresponding to pOA9). These data dem-

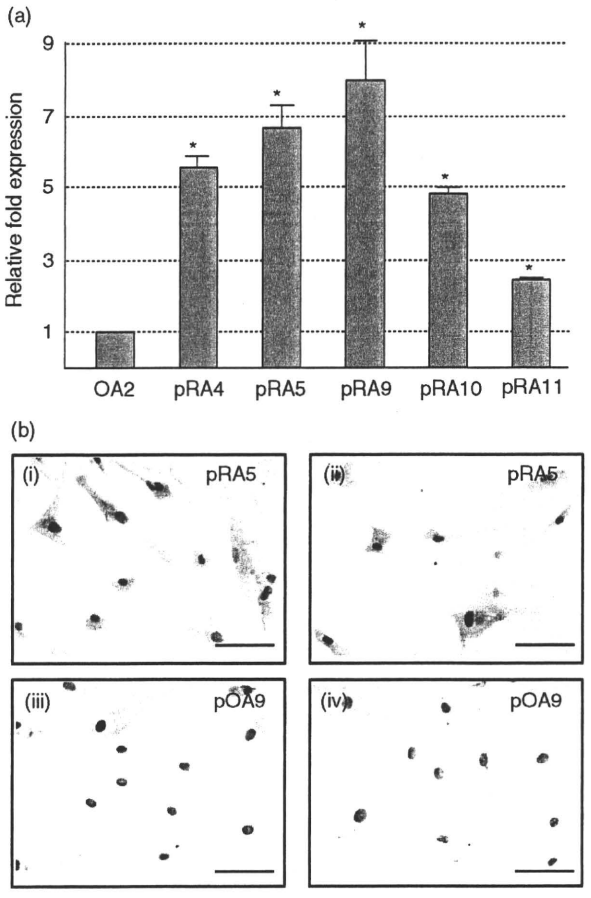

Fig. 4. Endogenous expression of activation-induced cytidine deaminase (AID) in non-transformed primary rheumatoid arthritis-fibroblast-like synoviocytes (RA-FLS). The identical number of primary FLS corresponding to that of transformed FLS indicates that both are derived from the same patient, except for pRA10 and pRA11, which have no corresponding transformants. (a) The expression level of *AID* was estimated and compared between transformed osteoarthritis (OA2) as control and non-transformed primary RA-FLS by real-time polymerase chain reaction (PCR). Relative fold expression was determined by the *AID* expression in OA2 being defined as 1. The grey bars and error bars indicate the averages and standard deviations, respectively, of two independent experiments. Asterisks indicate the statistically significant difference by Student's *t*-test. *P*-value < 0·01. Uncapitalized *p* at the head of RA means 'primary'. (b) Primary FLS grown on the glass slide were stained with rabbit anti-AID polyclonal antibody used in Western blot analysis (i and iii) or rat anti-AID monoclonal antibody (mAb) (ii and iv) combined with horseradish peroxidase-conjugated second antibodies. Diaminobenzidine was used as chromogenic substrate. Primary FLS cells from the same source of RA5 (i and ii, pRA5) and of OA9 (iii and iv, pOA9) are shown. Nuclear staining was performed with haematoxylin (violet). Scale bar indicates 100 μm.

onstrated clearly that the ectopic production of AID in RA-FLS is not a secondary effect by SV40 transformation.

Next, to examine whether AID production by RA-FLS is not the artefact *in vitro*, but the real event in the RA synovium *in situ*, we conducted immunohistochemical staining on the serial sections of the synovium from AID$^+$ RA patients with anti-CD20, anti-AID and control antibodies. The localization of CD20$^+$ B cells clearly isolated the follicles in the synovium (Fig. 5a, d), with a low frequency of AID-positive B cells. However, the majority of cells reacted by anti-AID antibody localized clearly in the lining and sublining outside the follicles (Fig. 5b, e). Isotype-matched irrelevant antibody towards mouse CD4 showed no signal on the serial specimen (Fig. 5c, f). Larger magnification revealed that AID signals were raised mainly from CD20$^-$ non-B cells that are morphologically compatible with FLS (Fig. 5g, h, black arrows), and some signals are originated from CD20$^+$ B cells (Fig. 5g, h, red arrows). To ensure this finding, double immunofluorescence staining with anti-AID and -CD20 mAbs was performed. The reactivity of anti-AID mAb (green) was obvious only in the AID-positive synovial tissue (Fig. 6a, c) but not in the AID-negative tissue (Fig. 6b, d). In higher magnification (Fig. 6e), the distinct area consisting of the cells reactive only to anti-AID mAb (green) spread well outside the area containing CD20$^+$ cells (red). The cells expressing both molecules are yellow and marked with an arrowhead in the figure.

These results demonstrated clearly that the FLS in the RA synovial tissues produce AID, providing strong evidence that ectopic and aberrant expression of AID occurs in RA.

Discussion

We have demonstrated that AID is expressed preferentially in transformed FLS cell lines from RA patients and that *AID* expression was correlated with accumulation of mutations in p53 gene. TNF-α enhanced the transcription of *AID* in both RA- and OA-FLS, whereas physiological concentration of β-oestradiol enhanced it only in RA-FLS. The selective and enhanced expression of *AID* was also confirmed in primary, non-transformed RA-FLS. Furthermore, localization of AID production outside the B cell follicles was demonstrated in the RA synovium tissue, providing definitive evidence that *AID* is expressed aberrantly and ectopically in certain cases of RA synovium. Thus, AID is a novel and intriguing candidate for the cause of the p53 mutation that has been reported to contribute the tumour-like phenotypes of RA-FLS.

To see the effects of *TP53* mutations on SV40-transformed RA-FLS, we examined the cell number after 4 days' culture and the transcription levels of *IL-6* and *MMP-1* by real-time PCR analysis, both of which did not demonstrate any correlation with expression of *AID*. Despite the concomitant detection of *TP53* mutations with *AID* transcription in a fraction of RA-FLS, the cell lines did not exhibit any tumour-

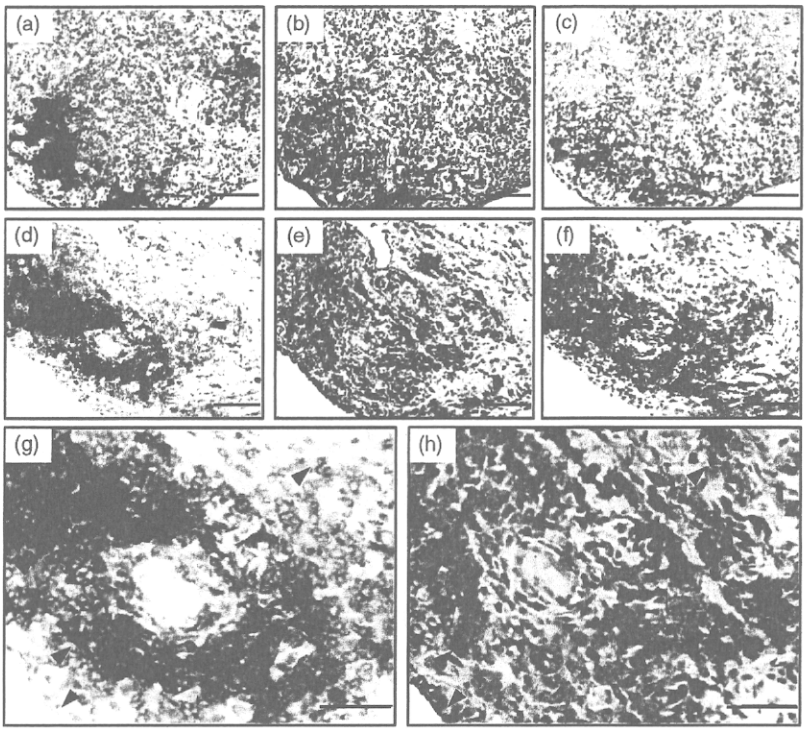

Fig. 5. Immunohistochemical studies of activation-induced cytidine deaminase (AID) expression on synovial tissue section from the representative rheumatoid arthritis (RA) patient. The (a) (d) and (g) sections were stained with anti-CD20 monoclonal antibody (mAb) to identify the location of the B cell-containing follicle in synovial tissue. The (b) (e) and (h) sections were with the rat mAb for AID, and (c) and (f) were with isotype-matched control antibody. The serial sections of (a) (b) and (c) were from RA4, and of (d) (e) and (f) were from RA5. The (g) and (h) sections were high-power fields corresponding to (d) and (e), respectively. Red and black arrows indicate B cells and non-B cells, respectively. Nuclear staining was performed with haematoxylin (violet). Scale bar indicates 100 μm.

like growth advantages or proinflammatory characteristics. However, this is plausible, because our sequence analyses could detect the generation of *TP53* mutations in the very low-frequent clones that are not sufficiently predominant to affect the characteristics of the *AID*^{high} RA-FLS line as a whole. Although not definitive, there was an informative and supportive RA case from which we obtained the two FLS lines from different joint lesions at distinct times of operation with a 6-month interval. Interestingly, AID expression was detectable only in the cell line established after the second operation, suggesting the possibility that ectopic expression of AID was acquired during the course of RA (unpublished observation). These intriguing possibilities should be tested using a larger sample size of clinical cases and/or quantitative histological analyses.

Xu *et al.* reported that B cells in the follicle of synovium or in the peripheral blood from RA patients show a higher expression level of AID in comparison with OA patients

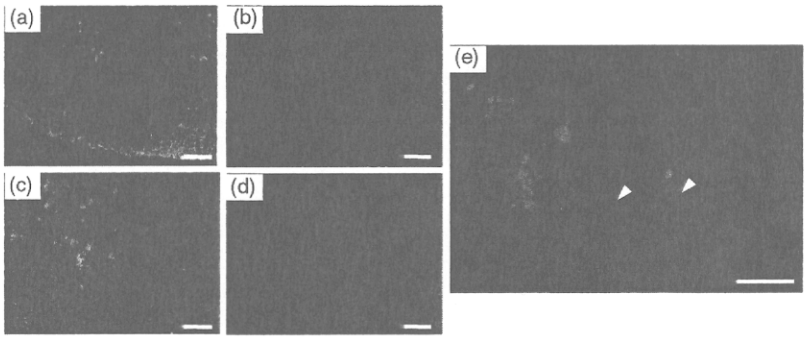

Fig. 6. Immunofluorescence staining of activation-induced cytidine deaminase (AID) on synovial tissue sections from the representative rheumatoid arthritis (RA) patient. All sections were stained with rat monoclonal antibody (mAb) for AID and anti-CD20 mAb simultaneously. AID was visualized with Alexa 488 fluoro-dye-conjugated anti-rat secondary antibody (green) and CD20 was visualized with Alexa 594 fluoro-dye-conjugated anti-mouse secondary antibody (red) and observed under fluoresence microscope. The sections of (a) were from an AID-positive RA sample corresponding to RA4, and of (b) was from another AID-negative RA sample from which no transformed cell line had been established. The sections of (c) and (e) were high-power fields corresponding to (a), and (d) were high-power fields corresponding to (b). White arrowheads indicate the cells expressing both AID and CD20. Nuclear staining was performed with 4,6-diamidino-2-phenylindole (violet). Scale bar indicates 100 μm in (a) and (b), 50 μm in (c) (d) and (e).

[40]. Our analyses in this paper demonstrated selective expression of AID in both transformed and non-transformed FLS from RA. Furthermore, immunohistochemical analysis of our RA cases revealed that major AID-producing cells with FLS-like morphology localized in the area outside B cell follicles; B cell follicles without production of AID were also described by them. When these results by us and others are integrated, we hypothesize that both B cells and non-B cells in RA patients are liable to express AID as an intrinsic or secondary abnormality under inflammatory milieu, which is responsible for the various aspects in the pathophysiology of RA. Higher expression of AID in B cells causes the SHM at variable regions in *Ig* gene and involvement in the generation of autoreactive B cells, which produce autoantibodies such as RF and anti-CCP antibody. Conversely, ectopic expression of AID in non-B cells, such as FLS *per se*, introduces point mutations in some genes, including tumour suppressor genes, and alters the phenotype of the cells including FLS.

It may be imagined that AID could be a potential therapeutic target for RA; however, it would be difficult to know when AID expression has begun in FLS in the synovium of each RA case. Although we did not study in detail the triggers for the ectopic expression of *AID* in FLS of RA, it is reasonable to speculate that anti-inflammatory cytokine therapy starting at earlier stages of RA suppresses the induction of AID expression in FLS and might prevent the malignant transformation of FLS by AID-dependent random mutagenesis.

Acknowledgements

We thank Ms Reina Tanaka for her technical assistance. We also thank Dr Kazuhiko Kuwahara at Kumamoto University for providing us with the SW480 colorectal cancer cell line, which was used for the positive control on APOBEC1 amplification. This work was supported by Research Project Grants (20-418I to H.I. and 19-406M to K.I.) from Kawasaki Medical School and Grants-in-Aid for Scientific Research from the Ministry of Education, Science, Sports, Culture and Technology of Japan (19590390 to K.I.).

Disclosure

None.

References

1 Lipsky PE. Rheumatoid arthritis. In: Fauci AS, Braunwald E, Kasper DL *et al.*, eds. Harrison's principles of internal medicine, 17th edn. New York: McGraw-Hill Professional, 2008:2083–91.

2 Firestein GS. Evolving concepts of rheumatoid arthritis. Nature 2003; **423**:356–61.

3 Mor A, Abramson SB, Pillinger MH. The fibroblast-like synovial cell in rheumatoid arthritis: a key player in inflammation and joint destruction. Clin Immunol 2005; **115**:118–28.

4 Kirkham BW, Lassere MN, Edmonds JP *et al.* Synovial membrane cytokine expression is predictive of joint damage progression in rheumatoid arthritis: a two-year prospective study (the damage study cohort). Arthritis Rheum 2006; **54**:1122–31.

5 Miossec P, Korn T, Kuchroo VK. Interleukin-17 and type 17 helper t cells. N Engl J Med 2009; **361**:888–98.

6 Andersson AK, Li C, Brennan FM. Recent developments in the immunobiology of rheumatoid arthritis. Arthritis Res Ther 2008; **10**:204.

7 Feldmann M, Brennan FM, Maini RN. Role of cytokines in rheumatoid arthritis. Annu Rev Immunol 1996; **14**:397–440.

8 McInnes IB, Schett G. Cytokines in the pathogenesis of rheumatoid arthritis. Nat Rev Immunol 2007; **7**:429–42.

9 Nishimoto N, Kishimoto T. Interleukin 6: from bench to bedside. Nat Clin Pract Rheumatol 2006; **2**:619–26.

10 Brennan FM, McInnes IB. Evidence that cytokines play a role in rheumatoid arthritis. J Clin Invest 2008; **118**:3537–45.

11 Firestein GS. Biomedicine. Every joint has a silver lining. Science 2007; **315**:952–3.

12 Pierer M, Muller-Ladner U, Pap T, Neidhart M, Gay RE, Gay S. The SCID mouse model: novel therapeutic targets – lessons from gene transfer. Springer Semin Immunopathol 2003; **25**:65–78.

13 Roivainen A, Pirila L, Yli-Jama T, Laaksonen H, Toivanen P. Expression of the myc-family proto-oncogenes and related genes max and mad in synovial tissue. Scand J Rheumatol 1999; **28**:314–18.

14 Aikawa Y, Morimoto K, Yamamoto T *et al.* Treatment of arthritis with a selective inhibitor of c-fos/activator protein-1. Nat Biotechnol 2008; **26**:817–23.

15 Firestein GS, Echeverri F, Yeo M, Zvaifler NJ, Green DR. Somatic mutations in the p53 tumor suppressor gene in rheumatoid arthritis synovium. Proc Natl Acad Sci USA 1997; **94**:10895–900.

16 Reme T, Travaglio A, Gueydon E, Adla L, Jorgensen C, Sany J. Mutations of the p53 tumour suppressor gene in erosive rheumatoid synovial tissue. Clin Exp Immunol 1998; **111**:353–8.

17 Kullmann F, Judex M, Neudecker I *et al.* Analysis of the p53 tumor suppressor gene in rheumatoid arthritis synovial fibroblasts. Arthritis Rheum 1999; **42**:1594–600.

18 Inazuka M, Tahira T, Horiuchi T *et al.* Analysis of p53 tumour suppressor gene somatic mutations in rheumatoid arthritis synovium. Rheumatology (Oxf) 2000; **39**:262–6.

19 Yamanishi Y, Boyle DL, Green DR *et al.* P53 tumor suppressor gene mutations in fibroblast-like synoviocytes from erosion synovium and non-erosion synovium in rheumatoid arthritis. Arthritis Res Ther 2005; **7**:R12–R18.

20 Pap T, Franz JK, Hummel KM, Jeisy E, Gay R, Gay S. Activation of synovial fibroblasts in rheumatoid arthritis: lack of expression of the tumour suppressor pten at sites of invasive growth and destruction. Arthritis Res 2000; **2**:59–64.

21 Han Z, Boyle DL, Shi Y, Green DR, Firestein GS. Dominant-negative p53 mutations in rheumatoid arthritis. Arthritis Rheum 1999; **42**:1088–92.

22 Yamanishi Y, Boyle DL, Rosengren S, Green DR, Zvaifler NJ, Firestein GS. Regional analysis of p53 mutations in rheumatoid arthritis synovium. Proc Natl Acad Sci USA 2002; **99**:10025–30.

23 Sun Y, Zeng XR, Wenger L, Firestein GS, Cheung HS. P53 down-regulates matrix metalloproteinase-1 by targeting the

communications between ap-1 and the basal transcription complex. J Cell Biochem 2004; **92**:258–69.
24 Goila-Gaur R, Strebel K. Hiv-1 vif, apobec, and intrinsic immunity. Retrovirology 2008; **5**:51.
25 Honjo T, Muramatsu M, Fagarasan S. Aid: how does it aid antibody diversity? Immunity 2004; **20**:659–68.
26 Di Noia JM, Neuberger MS. Molecular mechanisms of antibody somatic hypermutation. Annu Rev Biochem 2007; **76**:1–22.
27 Babbage G, Ottensmeier CH, Blaydes J, Stevenson FK, Sahota SS. Immunoglobulin heavy chain locus events and expression of activation-induced cytidine deaminase in epithelial breast cancer cell lines. Cancer Res 2006; **66**:3996–4000.
28 Endo Y, Marusawa H, Kinoshita K *et al.* Expression of activation-induced cytidine deaminase in human hepatocytes via nf-kappab signaling. Oncogene 2007; **26**:5587–95.
29 Kou T, Marusawa H, Kinoshita K *et al.* Expression of activation-induced cytidine deaminase in human hepatocytes during hepatocarcinogenesis. Int J Cancer 2007; **120**:469–76.
30 Endo Y, Marusawa H, Kou T *et al.* Activation-induced cytidine deaminase links between inflammation and the development of colitis-associated colorectal cancers. Gastroenterology 2008; **135**:889–98, 98 e1-3.
31 Komori J, Marusawa H, Machimoto T *et al.* Activation-induced cytidine deaminase links bile duct inflammation to human cholangiocarcinoma. Hepatology 2008; **47**:888–96.
32 Morisawa T, Marusawa H, Ueda Y *et al.* Organ-specific profiles of genetic changes in cancers caused by activation-induced cytidine deaminase expression. Int J Cancer 2008; **123**:2735–40.
33 Chan-On W, Kuwahara K, Kobayashi N *et al.* Cholangiocarcinomas associated with long-term inflammation express the activation-induced cytidine deaminase and germinal center-associated nuclear protein involved in immunoglobulin v-region diversification. Int J Oncol 2009; **35**:287–95.
34 Szczepek AJ, Bergsagel PL, Axelsson L, Brown CB, Belch AR, Pilarski LM. CD34+ cells in the blood of patients with multiple myeloma express CD19 and igh mrna and have patient-specific igh vdj gene rearrangements. Blood 1997; **89**:1824–33.
35 Pauklin S, Sernandez IV, Bachmann G, Ramiro AR, Petersen-Mahrt SK. Estrogen directly activates aid transcription and function. J Exp Med 2009; **206**:99–111.
36 Dorsett Y, McBride KM, Jankovic M *et al.* Microrna-155 suppresses activation-induced cytidine deaminase-mediated myc-igh translocation. Immunity 2008; **28**:630–8.
37 Teng G, Hakimpour P, Landgraf P *et al.* Microrna-155 is a negative regulator of activation-induced cytidine deaminase. Immunity 2008; **28**:621–9.
38 Shen HM, Poirier MG, Allen MJ *et al.* The activation-induced cytidine deaminase (aid) efficiently targets DNA in nucleosomes but only during transcription. J Exp Med 2009; **206**:1057–71.
39 Ko LJ, Prives C. P53: puzzle and paradigm. Genes Dev 1996; **10**:1054–72.
40 Xu X, Hsu HC, Chen J *et al.* Increased expression of activation-induced cytidine deaminase is associated with anti-ccp and rheumatoid factor in rheumatoid arthritis. Scand J Immunol 2009; **70**:309–16.

Mod Rheumatol (2011) 21:10–15
DOI 10.1007/s10165-010-0325-3

ORIGINAL ARTICLE

Humanized anti-interleukin-6-receptor antibody (tocilizumab) monotherapy is more effective in slowing radiographic progression in patients with rheumatoid arthritis at high baseline risk for structural damage evaluated with levels of biomarkers, radiography, and BMI: data from the SAMURAI study

Jun Hashimoto · Patrick Garnero · Désirée van der Heijde · Nobuyuki Miyasaka · Kazuhiko Yamamoto · Shinichi Kawai · Tsutomu Takeuchi · Hideki Yoshikawa · Norihiro Nishimoto

Received: 3 March 2010 / Accepted: 31 May 2010 / Published online: 24 June 2010

Abstract Our aim was to assess the ability of tocilizumab monotherapy to reduce progressive structural joint damage in rheumatoid arthritis patients at high risk of progression. This study was a subanalysis from a prospective 1-year, multicenter, X-ray-reader-blinded, randomized controlled trial of tocilizumab [Study of Active Controlled Monotherapy Used for Rheumatoid Arthritis, an IL-6 Inhibitor (SAMURAI) trial]. All patients were categorized into two or three groups according to four independent predictive markers for progressive joint damage [urinary C-terminal crosslinking telopeptide (uCTX-II), urinary pyridinoline/deoxypyridinoline (uPYD/DPD) ratio, body mass index (BMI), and joint-space narrowing (JSN) score at baseline]. One-year progression of joint destruction was assessed in high-risk versus low-risk groups receiving tocilizumab monotherapy and compared with patients receiving conventional disease-modifying antirheumatic drugs (DMARDs) ($n = 157$ and 145, respectively). In patients at high risk of progression of erosion as estimated by high uCTX-II, uPYD/DPD, or low BMI, and at high risk of progression of JSN as estimated by low BMI or high JSN score, the 52-week changes in radiological erosion and JSN, respectively, were significantly less in patients treated with tocilizumab monotherapy compared with those receiving DMARDs for each type of risk factor. In patients at low risk, those receiving tocilizumab also progressed less than those on DMARDs, although the difference did not reach statistical significance. Tocilizumab monotherapy is more effective in reducing radiological progression in patients presenting with risk factors for rapid progression than in low-risk patients. Patients at high risk for progression may benefit more from tocilizumab treatment.

Keywords CTX-II · PYD/DPD · Rheumatoid arthritis · Interleukin-6 · Tocilizumab · Joint destruction

J. Hashimoto · H. Yoshikawa
Osaka University Graduate School of Medicine, Osaka, Japan

P. Garnero
INSERM Research Unit 664, Lyon, France

D. van der Heijde
University Hospital Maastricht, Maastricht, The Netherlands

N. Miyasaka
Tokyo Medical and Dental University, Tokyo, Japan

K. Yamamoto
The University of Tokyo, Tokyo, Japan

S. Kawai
Toho University, Tokyo, Japan

T. Takeuchi
Keio University, Tokyo, Japan

N. Nishimoto
Wakayama Medical University, Wakayama, Japan

N. Nishimoto (✉)
Laboratory of Immune Regulation,
Wakayama Medical University, 105 Saito Bio Innovation Center, 7-7-20 Saito-Asagi, Ibaraki, Osaka 567-0085, Japan
e-mail: norichan@wakayama-med.ac.jp

Introduction

Biological agents targeting inflammatory cytokines have proven more effective than conventional disease-modifying antirheumatic drugs (DMARDs) for suppressing disease activity and progressive joint damage in rheumatoid arthritis (RA) [1–11]. Patients at high risk of progressive joint damage who are difficult to treat with conventional

DMARDs may be a particularly important target population for treatment with biologics. Our recent studies showed that increased urinary levels of C-terminal cross-linked telopeptide of type II collagen (uCTX-II), total pyridinoline/total deoxypyridinoline ratio (uPYD/DPD ratio), joint-space narrowing (JSN) score, and low body mass index (BMI) at baseline were all independent predictive markers for radiographically evident joint damage in patients with RA of <5 years and treated with conventional DMARDs. Although targeting patients with rapid progression, as assessed by these predictive factors, for treatment with biologics may be beneficial, to date there is no evidence that these agents are equally effective in such high-risk patients. Therefore, this study aimed to investigate the ability of tocilizumab monotherapy to reduce progressive structural joint damage in high-risk patients.

Methods

Patients with RA of <5 year duration participating in a prospective 1-year randomized controlled trial of tocilizumab [Study of Active Controlled Monotherapy Used for Rheumatoid Arthritis, an IL-6 Inhibitor (SAMURAI) trial] [10] receiving anti-interleukin (IL)-6-receptor antibody monotherapy (8 mg/kg intravenously every 4 weeks, $n = 154$), were categorized into two or three groups according to their uCTX-II values, uPYD/DPD ratio, BMI, and JSN scores at baseline (cutoff values: 500 ng/mmol creatinine for uCTX-II, median for uPYD/DPD, 0 units for JSN, 18.5 and 25 for BMI). These four factors were shown to be independent predictive markers for radiographically evident joint damage progression in 148 patients with RA treated with conventional DMARDs in the control arm of the SAMURAI trial [12]. Briefly, this trial established that high baseline uCTX-II, uPYD/DPD ratio and JSN score and a low BMI were independent risk factors for progression of bone erosion as evaluated with the van der Heijde modified Sharp method in patients with RA receiving conventional DMARDs. In addition to these three variables, the JSN score at baseline was also significantly associated with an increased risk of progression of JSN score and total Sharp score (TSS). In this study, we compared the 1-year progression of joint destruction in these high- and low-risk groups in the two cohorts of 148 and 154 patients with RA receiving conventional DMARDs or tocilizumab monotherapy, respectively.

SAMURAI trial

In the SAMURAI trial [10], patients were >20 years and fulfilled the American College of Rheumatology (ACR; formerly the American Rheumatism Association) 1987 revised criteria for the classification of RA, with a disease duration of ≥6 months and <5 years. In addition, they had ≥6 tender joints (of 49 evaluated), ≥6 swollen joints (of 46 evaluated), an erythrocyte sedimentation rate (ESR) of ≥30 mm/h, and C-reactive protein (CRP) of ≥20 mg/l. All patients had an inadequate response to at least one DMARD or immunosuppressant. Use of anti-tumor necrosis factor (anti-TNF) agents and leflunomide were not allowed within the 3 months prior to the first dose. Change in dose and type of DMARDs and/or immunosuppressants, plasma exchange therapies, and surgical treatments were not allowed within the previous 4 weeks. Oral corticosteroids (prednisolone up to 10 mg/day) were allowed if the dosage had not been changed during the prior 2 weeks. Patients were randomly assigned to receive either tocilizumab monotherapy at 8 mg/kg intravenously every 4 weeks or conventional DMARD therapy for 52 weeks. For the tocilizumab group, DMARDs and/or immunosuppressants were discontinued from the start of the study. Oral corticosteroids (up to 10 mg prednisolone per day) were allowed, but the dosage could not be increased during the study. Use of one nonsteroidal anti-inflammatory drug (NSAID), including switching to another NSAID, was allowed. For the conventional DMARD group, the dose, type, and combination of DMARDs and/or immunosuppressants, except for anti-TNF agents and leflunomide, could be varied according to disease activity at the discretion of the treating physician. Variations of NSAIDs and/or corticosteroids including intra-articular corticosteroid injections were also allowed.

Assessment of risk of radiographic progression

Posteroanterior radiographs of the hands and anteroposterior radiographs of the feet were acquired at baseline, week 28, and week 52 (or at the last visit for patients who withdrew from the study prior to week 52). Radiographs were scored using the van der Heijde modified Sharp method [13] for bone erosion, JSN, and TSS independently by two readers who were well trained and competent to score radiographs in accordance with the method. The readers were blinded to the treatment group and chronologic order of the images. We measured urinary total deoxypyridinoline (uDPD) and total pyridinoline (uPYD) by high-performance liquid chromatography (HPLC) and uCTX-II by enzyme-linked immunosorbent assay (ELISA) (CTX-II CartiLaps® ELISA, NORDIC Biosciences, Herlev, Denmark).

Statistical analysis

All statistical analyses were two-sided, and p values <0.05 were considered significant. All statistical analyses were carried out using SAS (SAS Institute, Cary, NC, USA version 8.2, TS2M0).

Results

Groups were comparable at baseline for the risk factors previously identified for predicting radiological progression in the DMARDs group (Table 1). As shown in Figs. 1 and 2, differences in the 1-year changes in radiological erosion and JSN scores between patients in the DMARDs and tocilizumab monotherapy arms varied between subgroups divided according to the baseline levels of each predictive marker for radiographically evident joint damage (uCTX-II, uPYD/DPD, JSN, and BMI). The 1-year changes in radiological erosion scores in patients with high uCTX-II, high uPYD/DPD, or low BMI at baseline, indicating a high risk of progressive joint erosion, were significantly lower in tocilizumab-treated than in DMARD-treated patients (Fig. 1). Those changes in radiological JSN scores in patients with high uCTX-II, high uPYD/DPD, high JSN, or low BMI at baseline, indicating a high risk of progressive JSN, were also lower in tocilizumab-treated than in DMARD-treated patients (Fig. 2a–d), and there were proven to be significant differences in cases with high JSN and low BMI (Fig. 2c, d). In contrast, low-risk patients receiving tocilizumab monotherapy progressed less than patients on DMARDs, although the differences were very small and did not reach statistical significance (Figs. 1 and 2).

Discussion

Biological agents targeting inflammatory cytokines are more effective at suppressing progression of joint damage than are conventional DMARDs. However, previously reported studies on the efficacies of these agents for slowing radiological damage showed that there was still significant progression in many patients [1–11]. These data allowed us to recognize that many patients on nonbiologic DMARDs show no radiographic progression, and some even show radiographic improvement. Specifically, our previous data showed that 39% of patients treated with conventional DMARDs showed no radiographic progression in 1-year follow-up [10]. However, biological agents may have side effects. With such knowledge gained from growing experience in the use of biologics, patients would benefit from personalized therapies based on accurate prognostic tools rather than standard therapies that do not evaluate risk factor to guide treatment selection. A better understanding of the prognostic factors for progressive joint damage under nonbiological treatment and appropriate targeting of biologics to patients with RA at high risk of progressive joint damage and disability could enhance risk–benefit balance of RA therapeutic strategies. Thus, many investigators have sought such prognostic factors. Young-Min et al. reported the possible usefulness of matrix metalloproteinase-3 (MMP-3) and uCTX-II in predicting radiographic outcome in RA patients treated with DMARDs [14], and Charni et al. reported the possible usefulness of urinary type II collagen helical peptide (HELIX-II) [15]. We found that high baseline levels of uCTX-II, uPYD/DPD, JSN score, and low BMI were independently significantly associated with 1-year progression of joint destruction under conventional DMARDs treatment [12]. Most of these newly developed or recognized markers are still not widely used in clinical practice; however, further understanding the significance of these markers would facilitate better therapies. Having established these risk factors, the efficacy of biologics for

Table 1 Baseline values in the different patient groups

Variables	Cutoff value	DMARDs $N = 145$		Tocilizumab $N = 157$	
		N	Mean of baseline value ± SD	*N*	Mean of baseline value ± SD
JSN	0	30	0	32	0
	>0	115	21.1 ± 22.5	125	18.2 ± 21.8
uCTX-II (ng/mmol/creatinine)	<500	53	327.2 ± 104.6	66	337.0 ± 102.9
	≥500	88	1249.0 ± 1014.9	83	1156.0 ± 585.8
uPYD/DPD	<6.8	72	5.8 ± 0.7	76	5.5 ± 0.8
	≥6.8	73	8.6 ± 1.4	81	8.5 ± 1.3
BMI (kg/m^2)	<18.5	20	17.5 ± 1.2	26	17.5 ± 0.6
	≥18.5 and <25	102	21.5 ± 1.6	102	21.5 ± 1.8
	≥25	21	27.1 ± 1.7	29	28.2 ± 2.4

Criteria were according to criteria of the World Health Organization [16] employees

JSN joint space narrowing, *uPYD/DPD* urinary pyridinoline/deoxypyridinoline ratio, *uCTX-II* urinary C-terminal telopeptide of type II collagen, *BMI* body mass index, *SD* standard deviation

BMI <18.5, underweight; ≥18.5 and <25, normal weight; 25≤, overweight or obese

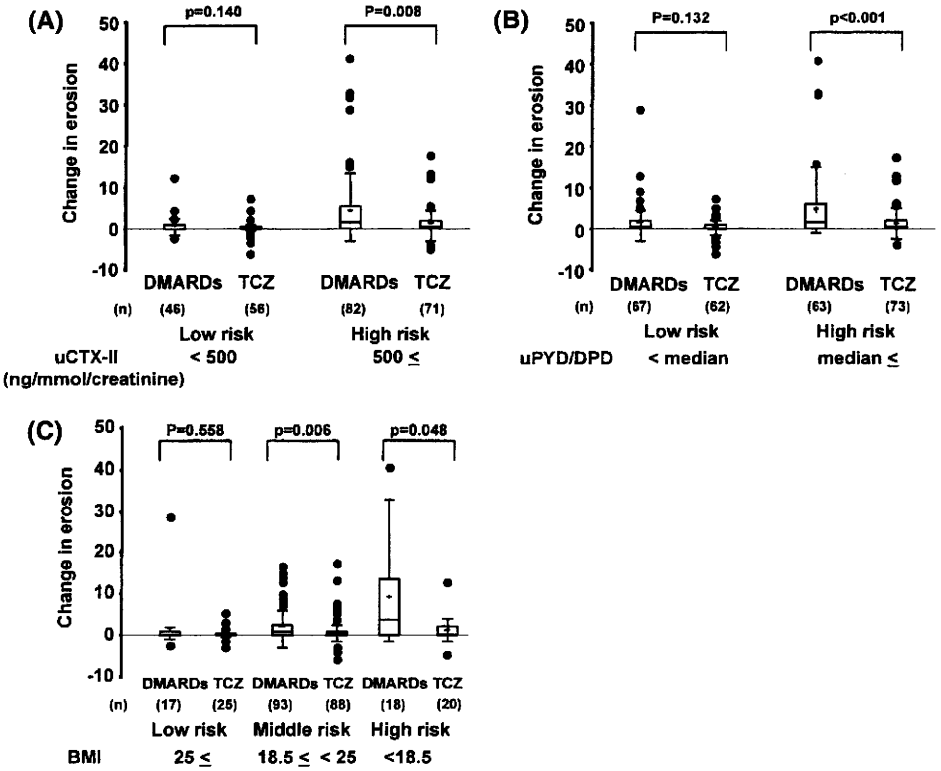

Fig. 1 One-year change of erosion scores in tocilizumab-treated rheumatoid arthritis (RA) patients at high risk for developing erosions. One-year change in erosion scores were analyzed for individual risk factors (**a** uCTX, **b** uPYD/DPD, **c** BMI) at baseline. Results are expressed as median (*line* across *boxes*), 25–75% interquartile range (*boxes*), mean (*cross symbol* in *boxes*), standard deviation (SD) (*vertical line* across the *top of the box*), and standard error (*vertical line* across *bottom of the box*). The *filled circles* represent individual values over SD values. Differences in changes in erosion scores were compared by the Wilcoxon rank sum test. *uPYD/DPD* urinary pyridinoline/deoxypyridinoline ratio, *uCTX-II* urinary C-terminal telopeptide of type II collagen, *BMI* body mass index, *TCZ* tocilizumab

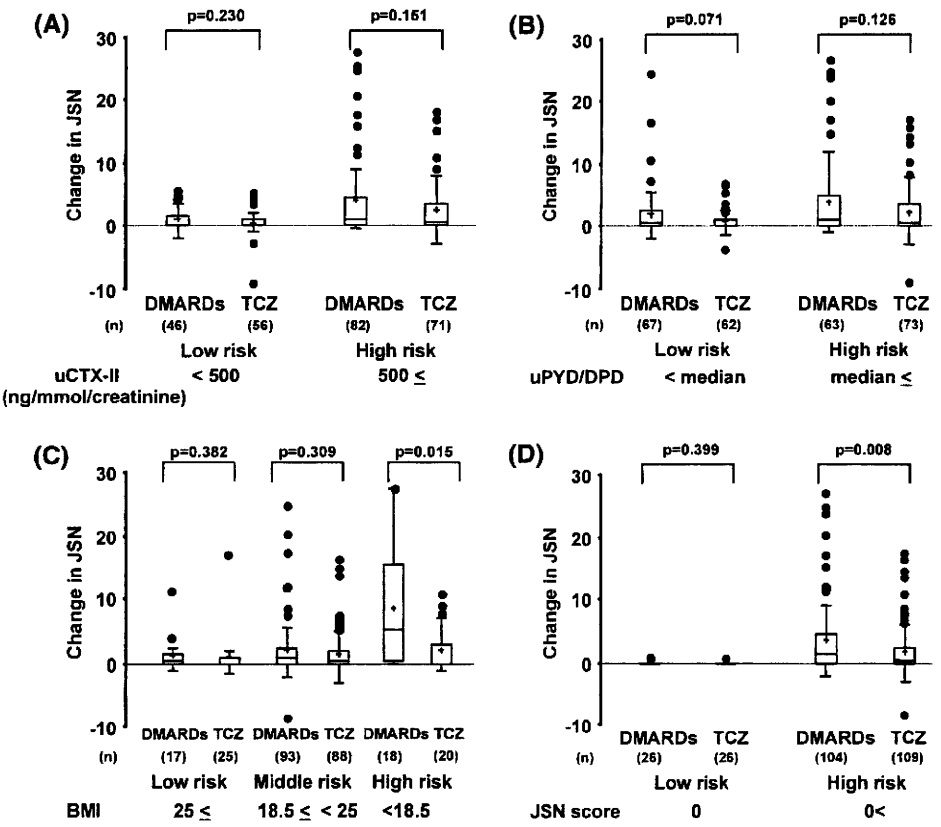

Fig. 2 One-year change of joint space narrowing (JSN) scores in tocilizumab-treated rheumatoid arthritis (RA) patients with risk factors for developing JSN. Score changes were analyzed for individual risk factors (**a** uCTX, **b** uPYD/DPD, **c** BMI, **d** JSN) at baseline. Results are expressed as median (*line* across *boxes*), 25–75% interquartile range (*boxes*), mean (*cross symbol* in *boxes*), standard deviation (SD) (*vertical line* across *top of the box*), and standard error (*vertical line* across *bottom of the box*). The *filled circles* represent individual values over SD values. Differences in change in JSN scores were compared by the Wilcoxon rank sum test. *uPYD/DPD* urinary pyridinoline/deoxypyridinoline ratio, *uCTX-II* urinary C-terminal telopeptide of type II collagen, *BMI* body mass index, *TCZ* tocilizumab

reducing joint destruction in high-risk groups needed to be confirmed to effectively target treatment. Therefore, in this study, subanalysis from a prospective 1-year randomized controlled trial of tocilizumab (SAMURAI trial) was performed to investigate the ability of this agent to reduce progression of structural joint damage in high-risk patients. There was no significant difference in 1-year changes of JSN scores between DMARD- and tocilizumab-treated patients in high-risk groups, as estimated by high uCTX-II, uPYD/DPD. Our data show, however, that tocilizumab monotherapy effectively blocked progression of bone erosion in all high-risk groups as estimated by high uCTX-II, uPYD/DPD, or low BMI and also effectively blocked progression of JSN in high-risk groups as estimated by low BMI or high JSN score, The differences in 1-year changes of erosion and JSN scores between the DMARD- and tocilizumab-treated patients were greatest in the high-risk groups, whereas there was little to no difference in the low-risk group. These findings indicate that the benefit of tocilizumab monotherapy to inhibit bone erosion and JSN progression is maximized in high-risk groups as estimated by high uCTX-II, uPYD/DPD, or low BMI, and by low BMI or high JSN score, respectively. To our knowledge, this is the first comprehensive report showing the usefulness of biomarker targeting strategies for biologics in treating RA. There were smaller and nonsignificant differences in 1-year changes of erosion and JSN scores between patients in the DMARD or tocilizumab monotherapy treatment groups in the low-risk category, although progression was still lower in individuals receiving tocilizumab. The lack of statistical significance can be due in part to the very limited progression in the low-risk group reducing the power to detect differences. These findings also suggest that patients at low risk may benefit less from treatment with biologics unless they develop changes in markers that indicate an increased risk of progression during treatment with conventional DMARDs. On the other hand, the lack of statistically significant differences in 1-year changes of JSN scores between patients in the DMARD or tocilizumab monotherapy treatment groups in the high-risk category might be due to the relatively weak prognostic power of high uCTX-II and uPYD/DPD for JSN progression compared with low BMI or high JSN score [12].

Establishing means of early discrimination between tocilizumab radiological responders and nonresponders is therefore raised as the next issue to be addressed when considering targeted therapeutic strategies. In conclusion, we demonstrated that tocilizumab monotherapy is effective in reducing radiological progression in patients presenting with risk factors for rapid progression of joint damage.

Acknowledgments This work was supported by Chugai Pharmaceutical Co., Ltd., Tokyo, Japan.

Conflict of interest statement NN has served as a consultant to and received honoraria from Chugai Pharmaceutical Co. Ltd., the manufacturer of TCZ. NN also works as a scientific advisor to F. Hoffmann-La Roche, which is developing TCZ in collaboration with Chugai Pharmaceutical Co., Ltd.

References

1. Lipsky PE, van der Heijde DM, St Clair EW, Furst DE, Breedveld FC, Kalden JR, et al. Infliximab and methotrexate in the treatment of rheumatoid arthritis. Anti-Tumor Necrosis Factor Trial in Rheumatoid Arthritis with Concomitant Therapy Study Group. N Engl J Med. 2000;343(22):1594–602.
2. Bathon JM, Martin RW, Fleischmann RM, Tesser JR, Schiff MH, Keystone EC, et al. A comparison of etanercept and methotrexate in patients with early rheumatoid arthritis. N Engl J Med. 2000; 343(22):1586–93.
3. Klareskog L, van der Heijde D, de Jager JP, Gough A, Kalden J, Malaise M, et al. Therapeutic effect of the combination of etanercept and methotrexate compared with each treatment alone in patients with rheumatoid arthritis: double-blind randomised controlled trial. Lancet. 2004;363(9410):675–81.
4. St Clair EW, van der Heijde DM, Smolen JS, Maini RN, Bathon JM, Emery P, et al. Combination of infliximab and methotrexate therapy for early rheumatoid arthritis: a randomized, controlled trial. Arthritis Rheum. 2004;50(11):3432–43.
5. Keystone EC, Kavanaugh AF, Sharp JT, Tannenbaum H, Hua Y, Teoh LS, et al. Radiographic, clinical, and functional outcomes of treatment with adalimumab (a human anti-tumor necrosis factor monoclonal antibody) in patients with active rheumatoid arthritis receiving concomitant methotrexate therapy: a randomized, placebo-controlled, 52-week trial. Arthritis Rheum. 2004;50(5): 1400–11.
6. Genovese MC, Bathon JM, Fleischmann RM, Moreland LW, Martin RW, Whitmore JB, et al. Longterm safety, efficacy, and radiographic outcome with etanercept treatment in patients with early rheumatoid arthritis. J Rheumatol. 2005;32(7):1232–42.
7. van der Heijde D, Landewe R, Klareskog L, Rodriguez-Valverde V, Settas L, Pedersen R, et al. Presentation and analysis of data on radiographic outcome in clinical trials: experience from the TEMPO study. Arthritis Rheum. 2005;52(1):49–60.
8. van der Heijde D, Klareskog L, Rodriguez-Valverde V, Codreanu C, Bolosiu H, Melo-Gomes J, et al. Comparison of etanercept and methotrexate, alone and combined, in the treatment of rheumatoid arthritis: two-year clinical and radiographic results from the TEMPO study, a double-blind, randomized trial. Arthritis Rheum. 2006;54(4):1063–74.
9. Breedveld FC, Weisman MH, Kavanaugh AF, Cohen SB, Pavelka K, van Vollenhoven R, et al. The PREMIER study: a multicenter, randomized, double-blind clinical trial of combination therapy with adalimumab plus methotrexate versus methotrexate alone or adalimumab alone in patients with early, aggressive rheumatoid arthritis who had not had previous methotrexate treatment. Arthritis Rheum. 2006;54(1):26–37.
10. Nishimoto N, Hashimoto J, Miyasaka N, Yamamoto K, Kawai S, Takeuchi T, et al. Study of active controlled monotherapy used for rheumatoid arthritis, an IL-6 inhibitor (SAMURAI): evidence of clinical and radiographic benefit from an x ray reader-blinded randomised controlled trial of tocilizumab. Ann Rheum Dis. 2007;66(9):1162–7.
11. Genant HK, Peterfy CG, Westhovens R, Becker JC, Aranda R, Vratsanos G, et al. Abatacept inhibits progression of structural

damage in rheumatoid arthritis: results from the long-term extension of the AIM trial. Ann Rheum Dis. 2008;67(8):1084–9.
12. Hashimoto J, Garnero P, van der Heijde D, Miyasaka N, Yamamoto K, Kawai S, et al. A combination of biochemical markers of cartilage and bone turnover, radiographic damage and body mass index to predict the progression of joint destruction in patients with rheumatoid arthritis treated with disease-modifying anti-rheumatic drugs. Mod Rheumatol. 2009;19(3):273–82.
13. van der Heijde D. How to read radiographs according to the Sharp/van der Heijde method. J Rheumatol. 2000;27(1):261–3.
14. Young-Min S, Cawston T, Marshall N, Coady D, Christgau S, Saxne T, et al. Biomarkers predict radiographic progression in early rheumatoid arthritis and perform well compared with traditional markers. Arthritis Rheum. 2007;56(10):3236–47.
15. Charni N, Juillet F, Garnero P. Urinary type II collagen helical peptide (HELIX-II) as a new biochemical marker of cartilage degradation in patients with osteoarthritis and rheumatoid arthritis. Arthritis Rheum. 2005;52(4):1081–90.
16. World Health Organization. Diet, nutrition and the prevention of chronic diseases. Report of a joint WHO/FAO expert consultation, January 28–February 1, 2002. Geneva: WHO; 2003. http://www.fao.org/DOCREP/005/AC911E/AC911E00.HTM

Bone 48 (2011) 476–484

Contents lists available at ScienceDirect

Bone

journal homepage: www.elsevier.com/locate/bone

PKCα suppresses osteoblastic differentiation

Akio Nakura, Chikahisa Higuchi *, Kiyoshi Yoshida, Hideki Yoshikawa

Department of Orthopaedic Surgery, Graduate School of Medicine, Osaka University, Suita, Osaka, Japan

ARTICLE INFO

Article history:
Received 11 May 2010
Revised 8 September 2010
Accepted 29 September 2010
Available online 14 October 2010

Edited by: Toshio Matsumoto

Keywords:
PKCα
MC3T3-E1 cells
Osteoblastic differentiation
Osteoblastic cell proliferation
Signal transduction

ABSTRACT

Protein kinase C (PKC) plays an essential role in cellular signal transduction for mediating a variety of biological functions. There are 11 PKC isoforms and these isoforms are believed to play distinct roles in cells. Although the role of individual isoforms of PKC has been investigated in many fields, little is known about the role of PKC in osteoblastic differentiation. Here, we investigated which isoforms of PKC are involved in osteoblastic differentiation of the mouse preosteoblastic cell line MC3T3-E1. Treatment with Gö6976, an inhibitor of PKCα and PKCβI, increased alkaline phosphatase (ALP) activity as well as gene expression of ALP and Osteocalcin (OCN), and enhanced calcification of the extracellular matrix. Concurrently, osteoblastic cell proliferation decreased at a concentration of 1.0 μM. In contrast, a PKCβ inhibitor, which inhibits PKCβI and PKCβII, did not significantly affect osteoblastic differentiation or cell proliferation. Knockdown of PKCα using MC3T3-E1 cells transfected with siRNA also induced an increase in ALP activity and in gene expression of ALP and OCN. In contrast, overexpression of wild-type PKCα decreased ALP activity and attenuated osteoblastic differentiation markers including ALP and OCN, but promoted cell proliferation. Taken together, our results indicate that PKCα suppresses osteoblastic differentiation, but promotes osteoblastic cell proliferation. These results imply that PKCα may have a pivotal role in cell signaling that modulates the differentiation and proliferation of osteoblasts.

Introduction

Protein kinase C (PKC) is a serine/threonine protein kinase that is known to be involved in multiple cellular signal transduction pathways that mediate cellular functions such as proliferation and differentiation [1–4]. PKC was first purified from bovine cerebellum in 1977 as a new species of protein kinase [5], following which, it was shown to be expressed in many other tissues [6]. To date, 11 PKC isoforms have been identified, which are classified into three groups based on their structure and cofactor regulation [7,8]: conventional PKC (α, βI, βII, and γ), novel PKC (δ, ε, η, θ, and μ), and atypical PKC (ζ and λ). Conventional PKCs are Ca^{2+}-dependent and are activated by both phosphatidylserine (PS) and the second messenger diacylglycerol (DAG). Novel PKCs are regulated by PS and DAG, but their activation is Ca^{2+}-independent. Atypical PKCs require neither Ca^{2+} nor PS and DAG for activation. Although some PKC isoforms are cell-type specific, PKCα, δ, ε, and ζ seem to be ubiquitous [7,9].

The role of each PKC isoform has been mostly evaluated in a variey of fields using genetic and molecular approaches employing isoform-specific inhibitors [10–12], isoform-specific RNAi and/or isoform overexpression. Much progress has been made in clinical studies of the role of PKC isoforms in cardiovascular disease and tumorigenesis and some isoforms of PKC are currently being used as theraupic targets [13]. For example, a selective inhibitor of PKCβ is under evaluation in a clinical trial as a theraupic agent for diabetic complications [14,15]. Although such systemic diseases often involve a change in bone quantity and quality, little is known about the effects of PKC on bone formation. Expression of PKC isoforms in osteoblasts has been reported [4,16], suggesting that a therapeutic agent targeted towards specific PKC isoforms might inadvertently modulate bone formation. Conversely, if the involvement of isoforms of PKC in bone formation are understood, a new agent for the regulation of bone formation might be developed.

Our purpose was to determine which isoforms of PKC play an important role in osteoblastic differentiation. In the present paper, we mainly investigated the role of PKCα and PKCβ in osteoblasts using commercially available inhibitors of PKC isoforms. We speculated that of the eleven different isoforms of PKC, PKCα in particular may have a suppressive role in osteoblastic differentiation. In addition, we confirmed this role of PKCα by knockdown of PKCα, and by overexpression of PKCα, in MC3T3-E1 cells. Meanwhile, PKCα promoted osteoblastic proliferation. Our present study indicates that PKCα suppresses osteoblastic differentiation.

* Corresponding author. Department of Orthopaedic Surgery, Graduate School of Medicine, Osaka University, 2-2 Yamadaoka, Suita, Osaka 565-0871, Japan. Fax: +81 6 6879 3559.
E-mail addresses: nakura-osaka@umin.ac.jp (A. Nakura), c-higuchi@umin.ac.jp (C. Higuchi), y_kiyoshi@csc.jp (K. Yoshida), yhideki@ort.med.osaka-u.ac.jp (H. Yoshikawa).

8756-3282/$ – see front matter © 2010 Elsevier Inc. All rights reserved.
doi:10.1016/j.bone.2010.09.238

Materials and methods

Cell culture

Mouse preosteoblastic MC3T3-E1 cells were obtained from Riken Cell Bank (Tsukuba, Japan). The cells were seeded at a concentration of 2.0×10^4 cells/cm^2 in α-minimal essential medium (α-MEM; Invitrogen, Carlsbad, CA, USA) supplemented with 10% fetal bovine serum (FBS; Hyclone, Road Logan, UT, USA) (growth medium) at 37 °C under a humidified atmosphere of 5% CO_2. For each assay, the growth medium was replaced with growth medium supplemented with 0.2 mM ascorbic acid (AA; Sigma-Aldrich, St. Louis, MO, USA) and 10 mM β-glycerophosphate (βGP; Sigma-Aldrich) (differentiation medium). The medium was changed twice per week.

Alkaline phosphatase (ALP) staining

MC3T3-E1 cells were seeded in a 24-well plate at a density of 2.0×10^4 cells/cm^2. After 24 h incubation, the cells were treated with the PKCα/PKCβI inhibitor Gö6976 (Calbiochem, San Diego, CA, USA), the PKCβ inhibitor (Calbiochem), or with 12-*O*-tetradecanoylphorbol-13-acetate (TPA; Calbiochem) in differentiation medium for 3 days. For ALP staining, cells were washed with phosphate-buffered saline (PBS; Sigma-Aldrich) and fixed for 15 min with 10% formalin at room temperature. After fixation, the cells were incubated with the ProtoBlot® II AP System with Stabilized Substrate (Promega, Madison, WI, USA) for 1 h at room temperature. For all experiments using inhibitors and activators of PKC, we also assayed the vehicle (DMSO) as a standard control [17].

ALP activity

To measure ALP activity, cells were washed twice with PBS and then lysed in mammalian protein extraction reagent (M-PER; Pierce, Rockford, IL, USA) following the manufacturer's protocol. ALP activity was measured using LabAssay™ ALP (Wako Pure Chemicals Industries, Ltd., Osaka, Japan) and p-nitrophenylphosphate as a substrate. In order to normalize enzyme activity, the protein content was measured using a bichinconinic acid (BCA) protein assay kit (Pierce).

Proliferation assay

MC3T3-E1 cells were cultured in 48-well plates at a concentration of 2.0×10^4 cells/cm^2 in differentiation medium. Cell proliferation was assessed using the Premix WST-1 cell proliferation assay system (Takara Bio, Inc., Otsu, Japan) according to the manufacturer's instructions. We performed this assay every 24 h.

Alizarin red staining

MC3T3-E1 cells were cultured for 28 days on BIOCOAT® 24-well plates (Nippon Becton Dickinson Co., Ltd., Tokyo, Japan) in differentiation medium. Then, the cells were washed twice with PBS, fixed in 10% formalin for 10 min and then stained with Alizarin Red S (Sigma-Aldrich) at pH 6.3 for 1 h. After discarding the Alizarin Red S solution and washing the cells three times with distilled water, bound Alizarin Red was dissolved in 200 μL of 100 mM hexadecylpyridium chloride (Sigma-Aldrich) and the absorbance of the supernatant was measured at 570 nm.

Reverse transcription PCR (RT-PCR) and quantitative real-time PCR

Total RNA was isolated from cells using TRIzol (Invitrogen) according to the manufacturer's instructions. cDNA was synthesized using the Transcriptor First Strand cDNA Synthesis kit (Roche Diagnostics GmbH, Mannheim, Germany). RT-PCR was performed using a PCR Master Mix (Promega) and an appropriate pair of primers. The sequences of the specific primers used for RT-PCR are shown in Table 1. PCR products were separated by agarose gel electrophoresis and stained with ethidium bromide. Each mRNA was measured using a quantitative real-time PCR assay, which employed LightCycler® TaqMan® Master (Roche Diagnostics), a Universal ProbeLibrary Probe (UPL Probe; Roche Diagnostics), an appropriate pair of primers according to the manufacturer's protocol. The sequences of specific primers and UPL Probes used are shown in Table 2. Expression values were normalized to GAPDH.

Western blotting

The cells were rapidly lysed on ice using Blue Loading Buffer Reagents (Cell Signaling Technology, Beverly, MA, USA) containing 0.125 M dithiothreitol. These samples were subjected to 8% SDS-PAGE and were then transferred onto nitrocellulose membranes (Bio-Rad Laboratories, Inc., Hercules, CA, USA). After blocking with 0.1% Tween-added PBS (T-PBS) containing 3% bovine serum albumin (BSA; Sigma-Aldrich), the membranes were incubated with specific primary antibodies against PKCα (Cell Signaling Technology), PKCβ (Abnova Co., Ltd., Taipei, Taiwan), PKCβII (Santa Cruz Biotechnology, Inc., Austin, TX, USA), and β-actin (Sigma-Aldrich). Horseradish peroxidase-conjugated anti-mouse or -rabbit secondary antibody (GE Healthcare, UK) were incubated for 1 h at room temperature in 0.1% T-PBS. The blots were visualized by enhanced chemiluminescence substrate (Thermo Scientific, Rockford, IL, USA) using a Western blotting detection system.

Knockdown of PKCα using RNA interference

MC3T3-E1 cells were transfected with small interfering RNA (siRNA) using Lipofectamine RNAiMAX (Invitrogen) according to the manufacturer's protocol. Two different sets of PKCα siRNA oligos were used for knockdown of PKCα: site 1 (5′-GGAUUUAUCUGAAGGCUGA-3′ and 5′-UCAGCCUUCAGAUAAAUCC-3′) and site 2 (5′-GCAAAGGACUUAUGACCAA-3′ and 5′-UUGGUCAUAAGUCCUUUGC-3′) (B-Bridge International, Inc., Sunnyvale, CA, USA). Control siRNA was purchased from B-Bridge International, Inc. MC3T3-E1 cells transfected with siRNA were seeded in a 24-well plate at a concentration of 1.0×10^4 cells/cm^2 for 48 h. The medium was then replaced with differentiation medium and the cells were incubated for 3 days prior to use for experiments.

Infection with adenovirus vectors

Adenovirus expressing rabbit PKCα, rabbit PKCβII, and β-galactosidase were generous gifts from Dr. M. Ohba, Tokyo, Japan [18]. Each recombinant adenovirus was plaque purified, expanded, and titered

Table 1
Sequences of PCR primers and specific probes used for quantitative real-time PCR.

Gene	UPL probe no.	Primer	Sequence (5′→3′)
ALP	81	Forward	ACTCAGGGCAATGAGGTCAC
		Reverse	CACCCGAGTGGTAGTCACAA
Osteocalcin	71	Forward	CACCATGAGGACCCTCTCTC
		Reverse	TGGACATGAAGGCTTTGTCA
Collagen type 1 a1	15	Forward	CATGTTCAGCTTTGTGGACCT
		Reverse	GCAGCTGACTTCAGGGATGT
Runx2	34	Forward	GCCCAGGCGTATTTCAGAT
		Reverse	TGCCTGGCTCTTCTTACTGAG
Osterix	106	Forward	CTCCTGCAGGCAGTCCTC
		Reverse	GGGAAGGGTGGGTAGTCATT
GAPDH	80	Forward	TGTCCGTCGTGGATCTGAC
		Reverse	CCTGCTTCACCACCTTCTTG

Table 2
Sequences of PCR primers used to amplify each of genes in RT-PCR.

Gene	Primer	Sequence (5′→3′)
ALP	Forward	GCCCTCTCCAAGACATATA
	Reverse	CCATGATCACGTCGATATCC
Osteocalcin	Forward	CAAGTCCCACACAGCAGCTT
	Reverse	AAAGCCGAGCTGCCAGAGTT
Collagen type 1 a1	Forward	GCAATCGGGATCAGTACGAA
	Reverse	CTTTCACGCCTTTGAAGCCA
Runx2	Forward	GCTTGATGACTCTAAACCTA
	Reverse	AAAAAGGGCCCAGTTCTGAA
Osterix	Forward	GAAGAAGCTCACTATGGCTC
	Reverse	GAAAAGCCAGTTGCAGACGA
GAPDH	Forward	TGAACGGGAAGCTCACTGG
	Reverse	TCCACCACCCTGTTGCTGTA

in 293 cells (Riken Cell Bank). MC3T3-E1 cells were infected and 2 days later, the medium was replaced with differentiation medium.

Statistical analysis

All data are expressed as means ± SD and a minimum of three independent experiments were performed for each assay. A two-sided unpaired Student's *t*-test, or analysis of variance (ANOVA) for multiple comparisons, was used for statistical analysis. A statistical difference between experimental groups was considered to be significant when the p value was <0.05.

Results

Osteoblastic differentiation of MC3T3-E1 cells is promoted by the PKCα/PKCβI inhibitor Gö6976

Prior to determination of the effects of PKC isoforms on osteoblastic differentiation, we first evaluated the endogenous expression of the PKC isoforms PKCα and PKCβ in MC3T3-E1 cells by western blotting. The expression of PKCα was identified in MC3T3-E1 cells. On the other hand, the expression of PKCβ, which indicates both PKCβI and PKCβII, was almost unidentified in MC3T3-E1 cells (Fig. 1A). We next investigated the effects of the expressed PKCs on osteoblastic differentiation by assay of the effect of incubation of MC3T3-E1 cells with various concentrations of the PKCα/PKCβI inhibitor Gö6976 (0–1.0 μM) for 72 h on ALP staining. In MC3T3-E1 cells, treatment with Gö6976 strongly induced ALP staining in a dose-dependent manner and also enhanced ALP activity (Fig. 1B). Furthermore, Alizarin Red S staining indicated that Gö6976 clearly promoted calcification of the extracellular matrix (ECM) in MC3T3-E1 cells. The degree of this ECM calcification was quantified by measurement of the absorbance of the Alizarin Red S solution (Fig. 1C). Quantitative real-time PCR assay showed acceleration of the mRNA expression of osteoblastic differentiation markers, including ALP, OCN, and Col1a1, and of the transcription factor Runx2, by Gö6976 in a dose-dependent manner (Fig. 1D). These findings indicate that Gö6976 promoted osteoblastic differentiation in MC3T3-E1 cells suggesting that the PKCα and/or PKCβI isoforms might have a suppressive effect on osteoblastic differentiation in MC3T3-E1 cells.

Treatment with the PKCβ inhibitor does not promote osteoblastic differentiation in MC3T3-E1 cells

To investigate which PKC isoform modulates osteoblastic differentiation, we examined the contribution of PKCβ to differentiation using a specific PKCβ inhibitor, which inhibits both PKCβI and PKCβII. Treatment of MC3T3-E1 cells with this PKCβ inhibitor had no influence on ALP activity (Fig. 2A). Moreover, neither calcification of the ECM (Fig. 2B), nor the expression of mRNA related to osteoblastic differentiation (Fig. 2C), changed in the presence of different concentrations of the PKCβ inhibitor. The inhibitor also induced no change in osteoblast-cell proliferation (data not shown). These data indicated that PKCβ, whether it is the PKCβI or PKCβII isoform, did not affect osteoblastic differentiation or cell proliferation. We therefore assumed that inhibition of PKCα by Gö6976 promoted osteoblastic differentiation in MC3T3-E1 cells.

Knockdown of PKCα promotes osteoblastic differentiation

To further confirm the effects of PKCα inhibition on osteoblastic differentiation in MC3T3-E1 cells, we investigated changes in cell differentiation following knockdown of PKCα using an RNA interference method. Fig. 3A shows the low cellular expression level of PKCα, 48 h after transfection of two different anti-PKCα siRNAs (Fig. 3A). Knockdown of PKCα using either siPKCα-1 or siPKCα-2 caused the up-regulation of ALP activity and the acceleration of ECM calcification in MC3T3-E1 cells compared to cells transfected with control siRNA (Figs. 3B and C). Furthermore, quantitative real-time PCR analysis revealed that the gene expression of ALP and OCN was dramatically increased by knockdown of PKCα but not by treatment with control siRNA. Among the other genes tested, the expression of Col1a1 showed some tendency to increase following knockdown of PKCα. Furthermore, knockdown of PKCα increased the mRNA expression of both of the transcription factors Runx2 and Osterix (Figs. 3D, E). These results indicated that PKCα may suppress osteoblastic differentiation.

Activation of PKC by TPA attenuates osteoblastic differentiation in MC3T3-E1 cells

We next investigated the influence of PKC activation by TPA on osteoblastic differentiation. Treatment with TPA (0–10 nM), which activates not only PKCα but also other conventional PKC and novel PKC isoforms, caused a decrease in ALP activity in a dose-dependent manner (Fig. 4A). Activation of PKC by TPA did not stimulate calcification of the ECM in MC3T3-E1 cells (Fig. 4B). In addition, RT-PCR analysis and quantitative real-time PCR showed that the expression of osteoblastic differentiation markers such as ALP and OCN were clearly decreased following TPA treatment in a dose-dependent manner (Figs. 4C, D).

Adenoviral overexpression of PKCα suppresses osteoblastic differentiation in MC3T3-E1 cells

To further confirm the functional role of PKCα in osteoblasts, we performed adenoviral-mediated gene transfer of wild-type PKCα (Ad-PKCα) and PKCβII (Ad-PKCβII) into MC3T3-E1 cells. Following gene transfer, we then confirmed a high expression level of the Ad-PKCα and Ad-PKCβII proteins by western blotting (Fig. 5A). We next measured the proliferation of MC3T3-E1 cells infected with each of the adenovirus vectors Ad-PKCα, Ad-PKCβII or Ad-βgal (control). Compared with cells transfected with Ad-βgal, the proliferation of MC3T3-E1 cells infected with Ad-PKCα was significantly increased on Days 4 and 5 after transfection, while the proliferation of cells transfected with Ad-PKCβII was similar to that of Ad-βgal cells (Fig. 5B). The observed acceleration of the proliferation of Ad-PKCα-transfected MC3T3-E1 cells is consistent with a previous report that PKCα has a stimulatory effect on human osteoblastic proliferation [19]. In addition, the overexpression of PKCα, but not that of PKCβII, suppressed ALP activity compared to overexpression of Ad-βgal (Fig. 5C). Quantitative real-time PCR analysis showed that overexpression of PKCα also suppressed the mRNA expression of ALP, Col1a1, Runx2, and Osterix compared with Ad-βgal (Fig. 5D).

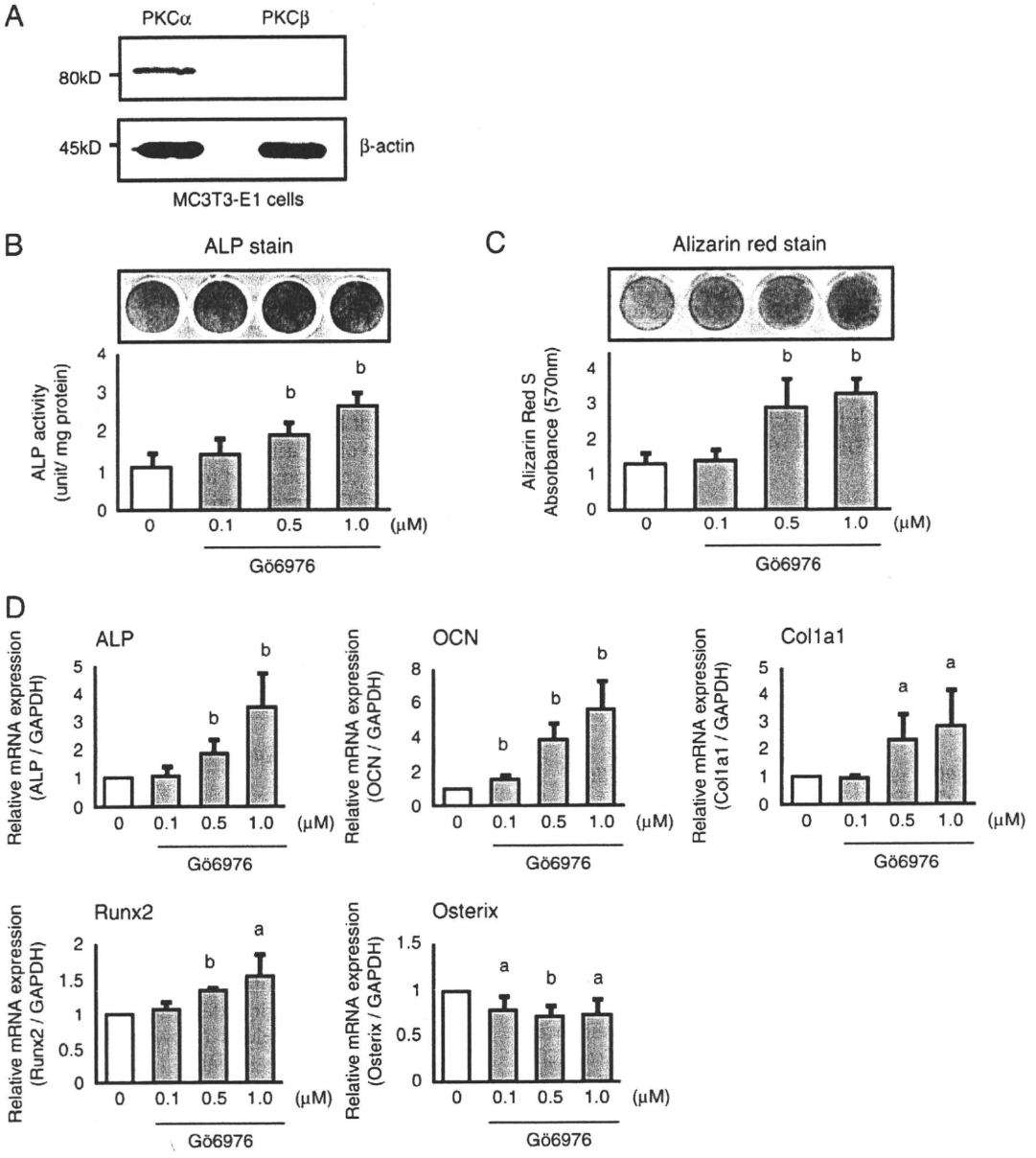

Fig. 1. Osteoblastic differentiation of MC3T3-E1 cells promoted by the PKCα/PKCβI inhibitor Gö6976. (A) endogenous expression of the PKCα, PKCβ proteins in MC3T3-E1 cells by western blotting. β-Actin was used as the internal control. (B) ALP staining and activity of MC3T3-E1 cells treated with Gö6976 which inhibits PKCα and PKCβI. MC3T3-E1 cells (2.0×10^4 cells/cm^2) were cultured in growth medium for 24 h, and then replaced with Gö6976 in differentiation medium for 3 days. (C) MC3T3-E1 cells stained with Alizarin red solution and quantified Ca content in the matrix of the cells. MC3T3-E1 cells were cultured with Gö6976 in differentiation medium for 28 days. Fresh medium was changed twice per week. (D) total RNA isolated from MC3T3-E1 cells treated with Gö6976 for 3 days. mRNA expression of the osteoblast-related genes: *ALP, OCN, Col1α1*; the transcription factor Runx2, and the gene *Osterix* was determined using quantitative real-time PCR analysis and UPL probes. The expression of each gene was normalized to GAPDH expression. (B, C, and D) data are means ± SD of three independent experiments performed in duplicate (a: $p<0.05$, b: $p<0.01$ compared with Gö6976-untreated control).

Discussion

In this study, we showed that PKCα has a suppressive effect on osteoblastic differentiation in MC3T3-E1 cells. Since the PKCα/PKCβI inhibitor Gö6976 accelerated ALP activity, and the PKCβ inhibitor had no influence on ALP activity, we concluded that PKCα is the PKC isoform that functions as a suppressor of osteoblastic differentiation. In addition, we confirmed which isoforms of PKC have specific effects on osteoblastic differentiation in ST2 cells, mouse bone marrow stromal cells. Although ST2 cells are more primitive than MC3T3-E1 cells, they are known to differentiate into osteoblast-like cells in differentiation medium in a similar manner to MC3T3-E1 cells [20]. Treatment of ST2 cells with Gö6976 increased ALP activity, with maximum activity observed at a concentration of 0.5 μM rather than at 1.0 μM, which was the concentration which gave maximum activation in MC3T3-E1 cells. Treatment of ST2 cells with the PKCβ inhibitor or TPA in did not alter ALP activity (data not shown). However, inhibition of PKCα also promoted osteoblastic differentiation in ST2 cells. Taken together, these results suggest that PKCα has a suppressive effect on osteoblastic differentiation that is not cell-type dependent. Thus, we focused on the role of PKCα in osteoblastic differentiation in MC3T3-E1 cells. Knockdown of PKCα promoted osteoblastic differentiation. In addition, calcification of ECM in MC3T3-E1 cells was also accelerated at 28 days after PKCα siRNA

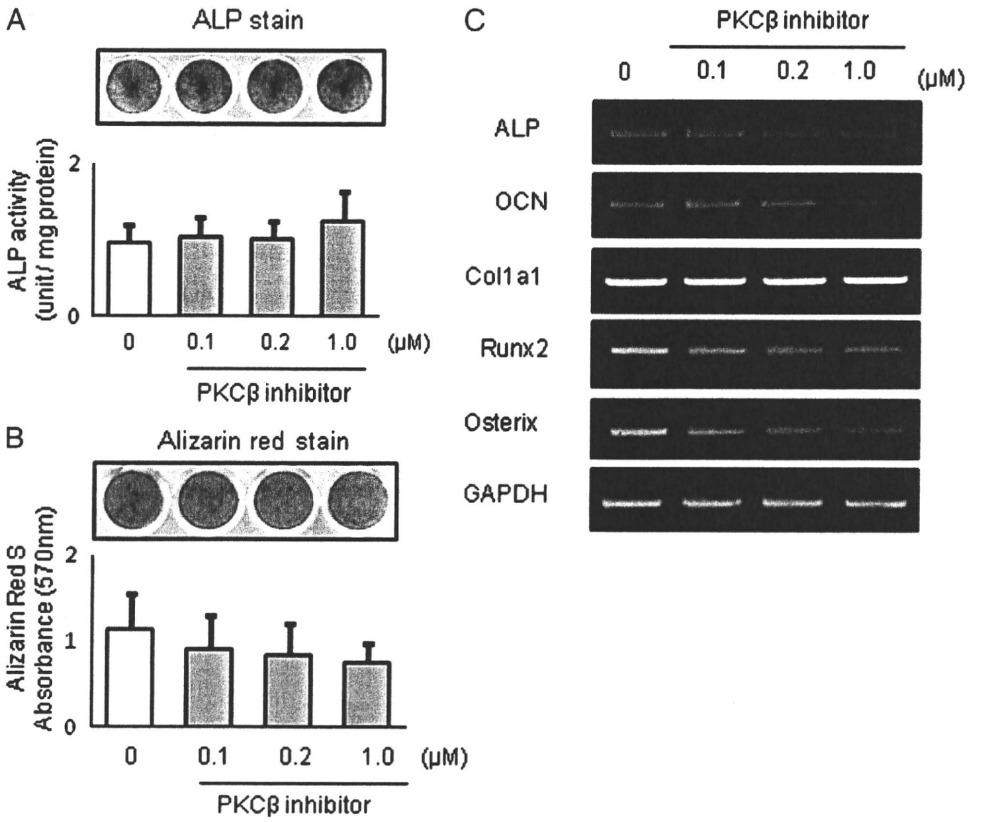

Fig. 2. Effect of PKCβ inhibitor on osteoblastic differentiation in MC3T3-E1 cells. (A) ALP staining and activity of MC3T3-E1 cells. The cells were cultured for 24 h, and then incubated for 3 days with PKCβ inhibitor in differentiation medium. (B) MC3T3-E1 cells stained with Alizarin red solution and quantified Ca content in the matrix of the cells. MC3T3-E1 cells were cultured with PKCβ inhibitor in differentiation medium for 28 days. Fresh medium was changed twice per week. (C) RT-PCR analysis of total RNA isolated from MC3T3-E1 cells treated with PKCβ inhibitor. Expression of osteoblastic related genes: ALP, OCN, Col1α1, Runx2, and Osterix. (A and B) data are means ± SD of three independent experiments performed in duplicate (a: $p<0.05$, b: $p<0.01$ compared with PKCβ inhibitor-untreated control).

transfection (Fig. 3C). In contrast, overexpression of PKCα decreased ALP activity (Fig. 5C) and reduced the expression of the mRNA of osteoblastic markers and transcription factors (Fig. 5D).

PKCα has been implicated in a number of biological functions such as proliferation, differentiation, cell cycle control, apoptosis/cell survival and cell adhesion [21]. In particular, PKCα is known to have an essential role in the proliferation of, not only osteoblasts [19], but also of other normal and tumor cells [22]. In the present study, we further demonstrated that PKCα has a role in the promotion of osteoblastic proliferation (Fig. 5B). Our data are in contrast to two previous reports of the involvement of PKCα in osteoblastic differentiation. Tang et al. [23,24] reported that PKCα is involved in the signal transduction pathway induced by basic fibroblast growth factor (bFGF) during stimulation of fibronectin expression in osteoblasts. The second previous report indicated that fibroblast growth factor receptor 2 (FGFR2) promotes osteogenic differentiation in mesenchymal cells via ERK1/2 and PKCα [25]. In these reports, PKCα was suggested to function in signal transduction pathways that promote osteoblastic differentiation. If PKCα can promote osteoblastic differentiation, inhibition of PKCα by Gö6976 and by PKCα siRNA should decrease osteoblastic differentiation. However, in this study, we showed that inhibition of PKCα promoted osteoblastic differentiation. Since we directly investigated PKCα using an inhibitor of PKCα as well as by knockdown and overexpression of PKCα, our results regarding the role of PKCα in osteoblastic differentiation may be more directly relevant to the cellular role of PKCα. Interestingly, Ogata et al. [26] reported that the G protein, $G\alpha_q$, activated PKC, and subsequently osteoblastic differention was suppressed. Although the isoform of PKC that was involved in the suppression of osteoblastic differentiation was not mentioned in that study, our data suggest the possibility that the results of Ogata might be due to a specific suppressive effect of the PKCα isoform.

Regarding the involvement of other isoforms of PKC in osteoblastic differentiation, there have been some reports that PKCδ activation promotes bone formation [27,28]. We found that treatment of MC3T3-E1 cells with Gö6983, which is an inhibitor of PKCα, β, γ, δ, and ζ, also enhanced ALP activity in a dose-dependent manner (data not shown). To completely rule out the possibility that PKCγ, δ, and ζ may also affect osteoblastic differentiation would require evaluation of the individual roles of PKCγ, δ, or ζ in differentiation. However, our data suggest that it is likely that inhibition of PKCα by Gö6983 strongly contributes to the promotion of ALP activity. Furthermore, PKCα may have a stronger influence on osteoblastic differentiation than PKCδ. Based on the IC_{50} values (half maximal inhibitory concentration) obtained using Gö6983, Gö6983 inhibits PKCα and PKCδ to the same extent [11]. Nevertheless, inhibition of PKCα rather than PKCδ might induce an increase in ALP activity in MC3T3-E1 cells. These results suggest that of the eleven isoforms of PKC, PKCα might have the most important for osteoblastic differentiation. We additionally confirmed that PKCβ, whether it is PKCβI or PKCβII, had little effects on osteoblastic differentiation or cell proliferation. This lack of effect of PKCβ may be related to a lack of expression of PKCβ in osteoblasts, as PKCβ expression has been suggested to be limited to specific tissues such as pancreatic islet cells,monocytes and brain [29]. We suggest that cellular function of PKCα on osteoblasts is not replaced with that of PKCβ, most similar isoform of PKCα.

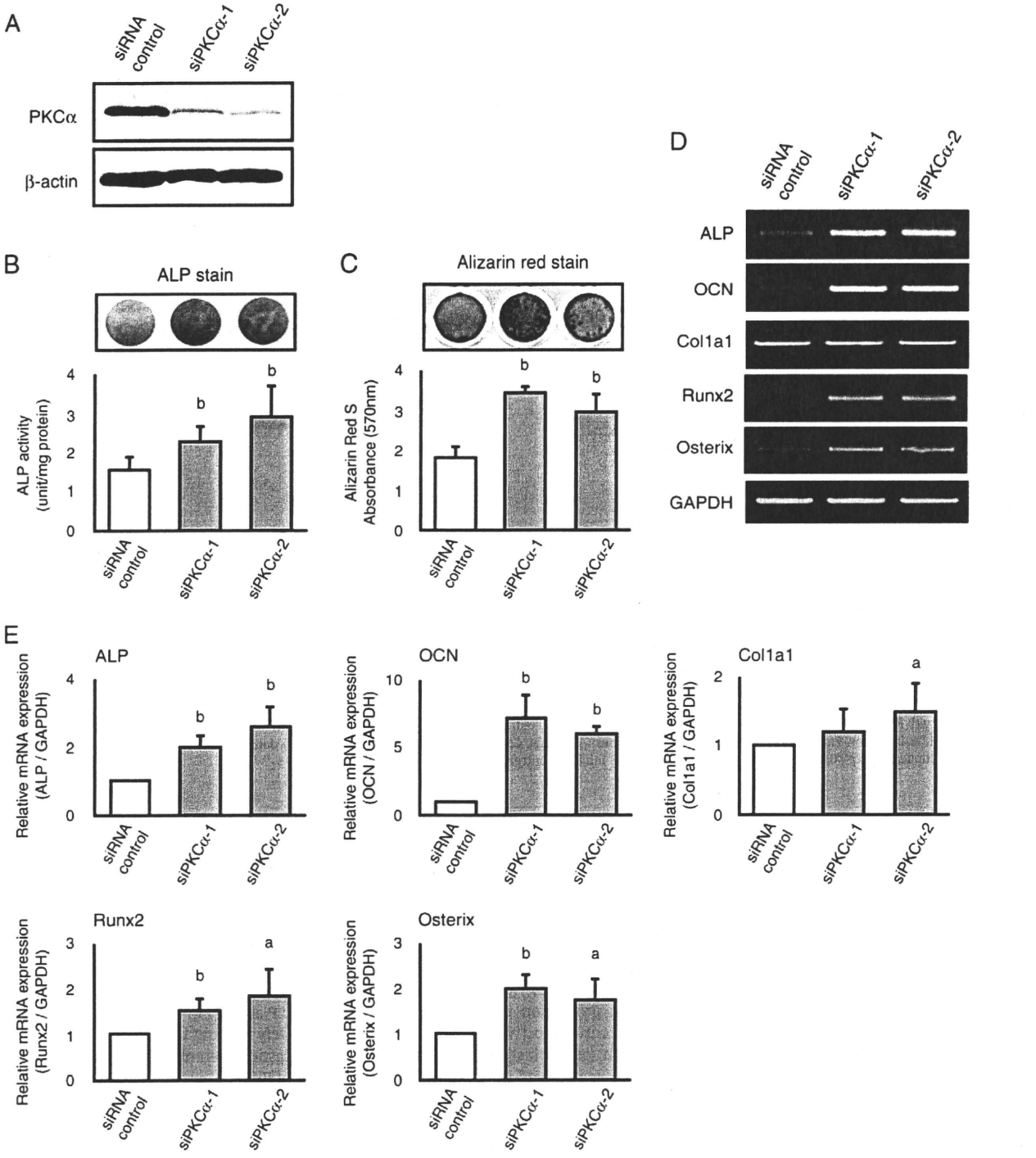

Fig. 3. Knockdown of PKCα stimulates osteoblastic differentiation. (A) Western blotting analysis of PKCα knockdown in MC3T3-E1 cells by transfection with control or PKCα (sites 1 and 2) siRNA. The cells transfected with siRNA were cultured for 48 h. Western blotting was performed using cell lysates as described in Materials and methods. (B) ALP staining and activity of MC3T3-E1 cells transfected with siRNA. The cells transfected with siRNA were incubated for 48 h, following which the medium was changed to differentiation medium. The cells were then incubated for 3 days to evaluate the osteoblastic differentiation. (C) Alizarin red staining and quantified Ca content. MC3T3-E1 cells transfected with control and PKCα siRNA were cultured and incubated in growth medium for 2 days, and then replaced in differentiation medium for 28 days. Fresh medium was changed twice per week. (D and E) expression of osteoblastic-related genes in MC3T3-E1 cells transfected with control and PKCα siRNA was assessed by RT-PCR and quantitative real-time PCR. Total RNA was extracted from MC3T3-E1 cells. The expression of each gene was normalized against GAPDH expression. (B, C, and E) Data are means ± SD of three independent experiments performed in duplicate (a: $p<0.05$, b: $p<0.01$ compared with siRNA control).

Signaling pathways activated downstream of PKCα have been reported to involve the p44/42 MAPK, which is activated by PKCα in various types of cells [19,30–33]. We therefore investigated whether p44/42 MAPK activation is regulated by inhibition of PKCα using the PKC inhibitor or by knockdown of PKCα using RNA interference, or by overexpression of PKCα using Ad-PKCα in MC3T3-E1 cells. However,

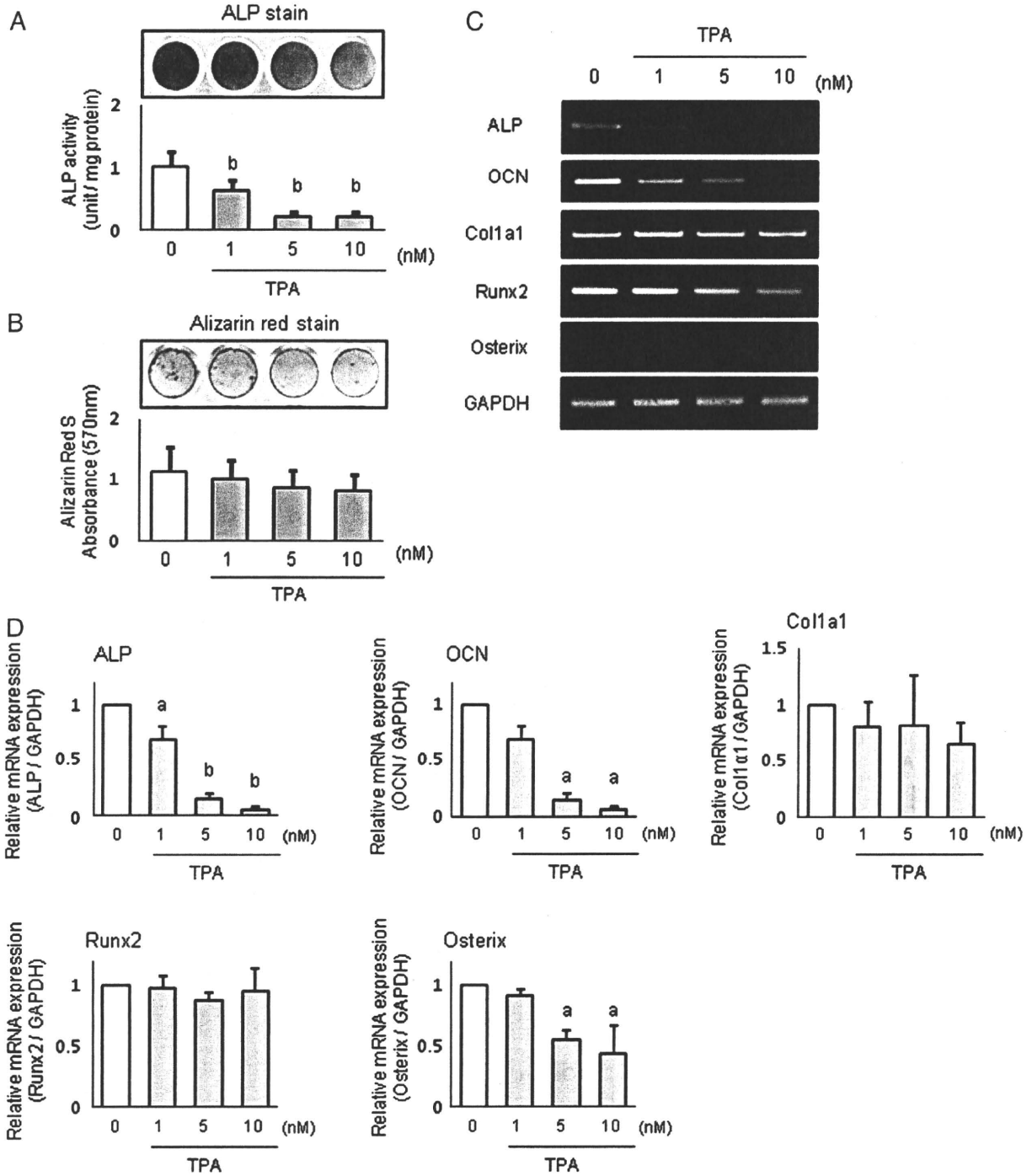

Fig. 4. Effect of TPA on osteoblastic differentiation in MC3T3-E1 cells. (A) ALP staining and activity of MC3T3-E1 cells. The cells were cultured for 24 h, and then incubated for 3 days after treatment with TPA in differentiation medium. (B) MC3T3-E1 cells stained with Alizarin red solution and quantified Ca content in the matrix of the cells. MC3T3-E1 cells were cultured with TPA in differentiation medium for 28 days. Fresh medium was changed twice per week. (C) RT-PCR analysis of total RNA isolated from MC3T3-E1 cells treated with TPA. Expression of osteoblastic-related genes: ALP, OCN, Col1α1, Runx2, and Osterix. (D) total RNA isolated from MC3T3-E1 cells treated with TPA for 3 days. mRNA expression of the osteoblast-related genes: *ALP, OCN, Col1α1*; the transcription factor Runx2, and the gene *Osterix* was determined using quantitative real-time PCR analysis and UPL probes. The expression of each gene was normalized to GAPDH expression. (A, B and D) data are means ± SD of three independent experiments performed in duplicate (a: $p<0.05$, b: $p<0.01$ compared with TPA-untreated control).

significant alteration of the phosphorylation of p44/42 MAPK, as assessed by western blotting, was not correlated with PKCα (data not shown). Interestingly, it is reported that p44/42 MAPK was activated by insulin sitimulation in vastus lateralis skeletal muscles even in a PKCα knockout mouse [34]. Since PKCα plays multiple roles in signal transduction and it does not directly activate p44/42 MAPK [35,36], it is possible that activation of downstream signal pathways other than modulation of p44/42 MAPK by inhibition of PKCα might lead to osteoblastic differentiation. Further study is required to elucidate the signal pathway downstream of PKCα during osteoblastic differentiation.

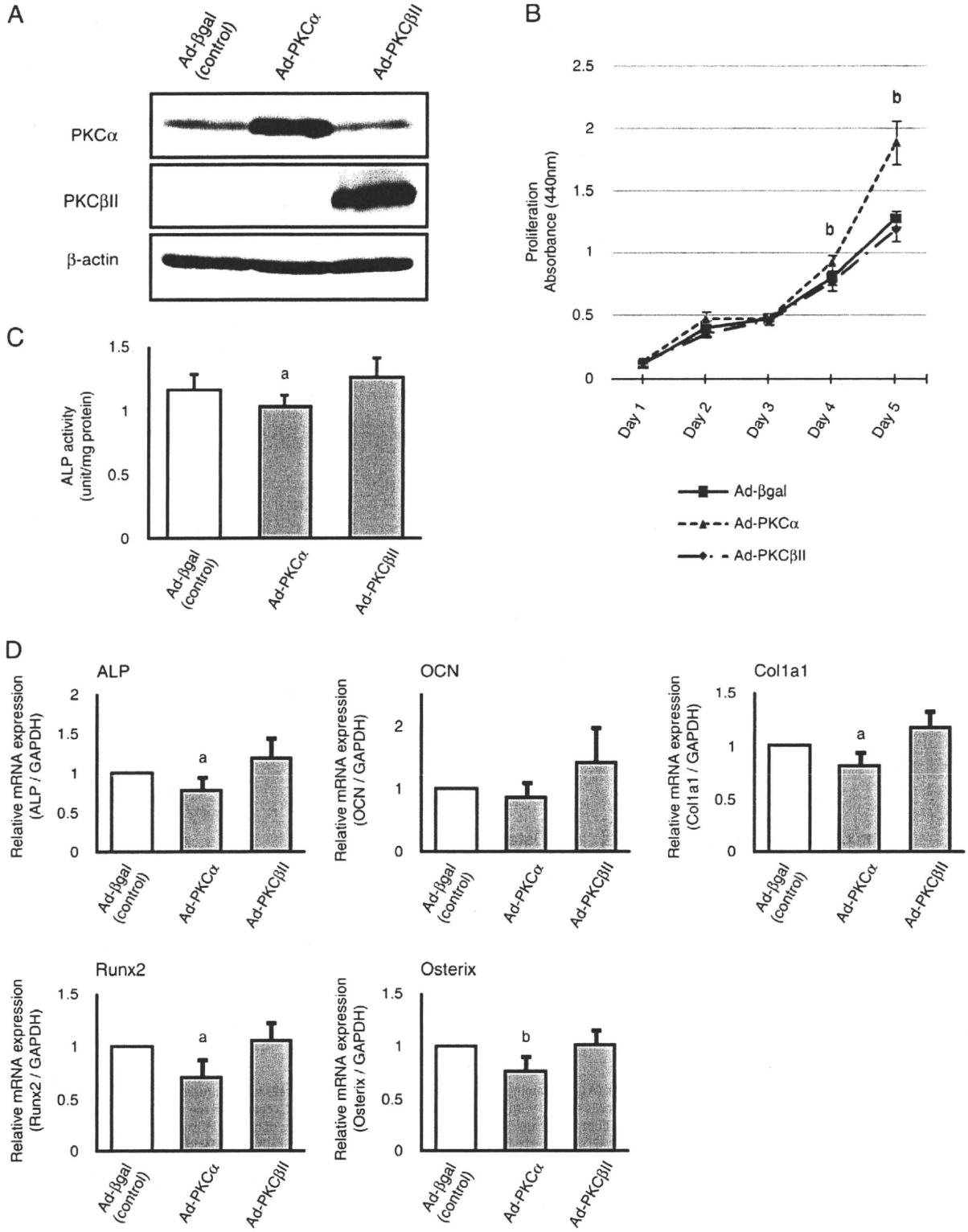

Fig. 5. Effects of PKCα overexpression on MC3T3-E1 cells. (A) Western blotting analysis of PKCα and PKCβII overexpression. Total cell lysates were extracted from MC3T3-E1 cells infected with adenovirus-encoding wild-type of PKCα, PKCβII. (B) proliferation of MC3T3-E1 cells infected with adenovirus encoding an empty vector, (Ad-βgal, control), wild-type PKCα (Ad-PKCα), or PKCβII (Ad-PKCβII). Infected MC3T3-E1 cells were incubated for 2 days following which the medium was changed to differentiation medium and the cells were incubated for a further 3 days. Cell proliferation was assayed at daily intervals over these 5 days of incubation. (C) ALP activity of MC3T3-E1 cells with PKCα overexpression. ALP activity was determined and normalized to the protein content. (D) expression of osteoblastic-related gene in MC3T3-E1 cells infected with Ad-βgal (control), Ad-PKCα, and Ad-PKCβII were assessed by real-time PCR analysis. Total RNA was extracted from MC3T3-E1 cells. (B, C, and D) Data are means ± SD of three independent experiments performed in duplicate (a: $p<0.05$, b: $p<0.01$ compared with Ad-βgal).